NTNU
Norwegian University of
Science and Technology

Passive Earth Pressures and Related Deformations of Bridge Abutments

Back Calculation of Passive Earth Pressure
Load Tests

Mari Melhus Romstad

Civil and Environmental Engineering
Submission date: June 2018
Supervisor: Arnfinn Johannes Emdal, IBM
Co-supervisor: Steinar Nordal, IBM
Lars Grande, Norconsult

Norwegian University of Science and Technology
Department of Civil and Environmental Engineering

NORGES TEKNISK-
NATURVITENSKAPELIGE UNIVERSITET
INSTITUTT FOR BYGG OG MILJØTEKNIKK

Report Title: **Passive Earth Pressures and Related Deformations of Bridge Abutments**	Date: **11.06.2018** Number of pages (incl. Appendices): **98**	
	Master Thesis	x

Name:
Mari Melhus Romstad

Professor in charge/supervisor:
Steinar Nordal

Other external professional contacts/supervisors:
Arnfinn Emdal

Abstract:
In this thesis the earth pressure theories developed by Rankine, Coulomb, Terzaghi and Janbu have been studied and used for hand calculations. The theories are based upon a series of simplifications and idealizations, and will therefore to a certain degree be inaccurate when compared to experimental results. The biggest limitations of the theories are that they implicitly assume the dilatancy angle ψ to be equal to the angle of friction φ, they do not account for the displacement of the wall, in addition to assuming linear horizontal stress distribution with depth. The research suggests that the Janbu theory provides the most accurate results for wall roughness r>0, while all the theories are suitable for calculations where r=0.

This study has consisted of back-calculations of passive loading tests using the Mohr-Coulomb and Hardening Soil Model in Plaxis 2D and Plaxis 3D. Two passive load tests have been back-calculated in order to gather experience on soil behaviour during passive loading. The results suggest that the stiffness parameters E' and E_{50}^{ref}, cohesion c_u or c and the friction angle φ are the most important parameters when modeling passive load tests in Plaxis. A critical evaluation of what values of φ to use in Plaxis simulations is recommended.. For cases where the backfill is compacted, the use of empirical values in the higher range is recommended. For uncompacted backfill empirical values in the lower range should be used. The author found that there is good agreement between the experimental load-deflection curves and the curves obtained from Plaxis when adjusting the angle of friction. In Case 1 a narrow wall was modeled, resulting in the 3D simulations being the most accurate. Case 2 consisted of a wide wall where the 2D and 3D simulations displayed similar accuracy. The effect of mesh density was found to be varying for the two cases, with the coarse mesh displaying a failure load overshoot of 7-12% compared to the very fine mesh in 2D, and 7-20% compared to the fine mesh in 3D. The relatively large overshoot in Plaxis 3D is partly due to the poor quality of the 10-node tetrahedral elements. For modeling of wide bridge abutments with plane strain conditions the research suggests that Plaxis 2D should be used, and using a fine mesh will provide accurate results. For narrow abutments Plaxis 3D will be more relevant, and the use of a medium mesh is recommended. When using a medium mesh an overshoot in the range of 5 to 10% is expected. For the reviewed cases the relation between wall height and horizontal displacement at failure was found to be approximately $\delta_h/H = 3\%$.

Keywords:

1. Passive Earth Pressure
2. Bridge Abutments
3. Back Calculation
4. Finite Element Analysis

Mari Melhus Romstad

Preface

This master thesis was carried out during the spring semester of 2018 at the NTNU, Trondheim. The work in this report represents 30 credits and completes my Master in Science degree in Civil and Environmental engineering. The master thesis has been written under the supervision of the Geotechnical department at NTNU, with Professor Steinar Nordal as main supervisor.

The idea behind the thesis was initiated by Norconsult, but the problem formulation has been modified several times throughout the process. The readers of this master thesis are assumed to have basic knowledge on soil mechanics.

Trondheim, 2018-06-11

Mari Melhus Romstad

Acknowledgment

I would like to express my gratitude to all the professors in the division of Geotechnics for giving me much help during the masters study. A big thanks goes also to Norconsult for providing me with the initial idea of the thesis.

Hereby I hope to especially thank my supervisor Professor Steinar Nordal for the great support and guidance during the project. He was ready to help whenever I had a question about my research or writing, and provided useful comments, remarks and engagement throughout the process.

The thesis writing would not have been the same without the company of my fellow students in the division of Geotechnics at NTNU. Thank you for the great conversations and support, and best of luck in the future.

M.M.R.

Abstract

In this thesis the earth pressure theories developed by Rankine, Coulomb, Terzaghi and Janbu have been studied and used for hand calculations. The theories are based upon a series of simplifications and idealizations, and will therefore to a certain degree be inaccurate when compared to experimental results. The biggest limitations of the theories are that they implicitly assume the dilatancy angle ψ to be equal to the angle of friction ϕ, they do not account for the displacement of the wall, in addition to assuming linear horizontal stress distribution with depth. The research suggests that the Janbu theory provides the most accurate results for wall roughness $r > 0$, while all the theories are suitable for calculations where $r = 0$.

This study has consisted of back-calculations of passive loading tests using the Mohr-Coulomb and Hardening Soil Model in Plaxis 2D and Plaxis 3D. Two passive load tests have been back-calculated in order to gather experience on soil behaviour during passive loading. The results suggest that the stiffness parameters E' and E_{50}^{ref}, cohesion c_u or c and the friction angle ϕ are the most important parameters when modeling passive load tests in Plaxis. A critical evaluation of what values of ϕ to use in Plaxis simulations is recommended. For cases where the backfill is compacted, the use of empirical values in the higher range is recommended. For poorly compacted backfill empirical values in the lower range should be used. The author found that there is good agreement between the experimental load-deflection curves and the curves obtained from Plaxis when adjusting the angle of friction. In Case 1 a narrow wall was modeled, resulting in the 3D simulations being the most accurate. Case 2 consisted of a wide wall where the 2D and 3D simulations displayed similar accuracy. The effect of mesh density was found to be varying for the two cases, with the coarse mesh displaying a failure load overshoot of 7-12% compared to the very fine mesh in 2D, and 7-20% compared to the fine mesh in 3D. The relatively large overshoot in Plaxis 3D is partly due to the poor quality of the 10-node tetrahedral elements. For modeling of wide bridge abutments with plane strain conditions the research suggests that Plaxis 2D should be used, and using a fine mesh will provide accurate results. For narrow abutments Plaxis 3D will be more relevant, and the use of a medium mesh is recommended. When using a medium mesh an overshoot in the range of 5 to 10% is expected. For the reviewed cases the relation between wall height and horizontal displacement at failure was found to be approximately $\delta_h/\mathrm{H} = 3\%$.

Sammendrag

I denne oppgaven har jordtrykksteorier utviklet av Rankine, Coulomb, Terzaghi og Janbu blitt forklart og brukt til håndberegninger. Teoriene er basert på flere forenklinger og vil derfor til en viss grad variere med virkeligheten. Teorienes største begrensninger er at de implisitt antar at dilatansvinkelen ψ er lik friksjonsvinkelen ϕ, de tar ikke hensyn til forskyvningen av veggen og de antar lineær horisontalspenningsfordeling med dybden. Resultatene indikerer at Janbus teori gir mest nøyaktige resultater for ruhet $r > 0$, mens alle teoriene kan benyttes når $r = 0$.

Tilbakeregning av lasttester med bruk av Mohr-Coulomb og Hardening Soil Model har blitt utført i Plaxis 2D og Plaxis 3D. To passive lasttester har blitt tilbakeregnet for å samle erfaring om jordoppførsel under passiv last. Resultatene antyder at stivhetsparameterne E' og E_{50}^{ref}, kohesjonen c_u eller c og friksjonsvinkelen ϕ er de viktigste parameterne når passive lasttester skal modelleres i Plaxis. Det anbefales å foreta en kritisk vurdering av hvilke verdier av ϕ som skal brukes i Plaxis. For tilfeller der fyllingen er kompaktert anbefales bruk av parametere i det høyere området av erfaringsverdier, og i tilfeller hvor fyllingen er dårlig kompaktert burde verdier i det lavere området benyttes. Det ble funnet god overensstemmelse mellom de eksperimentelle last-forskyvningskurvene og kurvene beregnet i Plaxis når friksjonsvinkelen blir justert. I Case 1 ble en smal vegg modellert, og de mest nøyaktige resultatene ble oppnådd gjennom 3D-simulering. I Case 2 ble en bred vegg modellert, og her viste 2D- og 3D-simuleringene tilnærmet lik nøyaktighet. Effekten av meshtetthet ble funnet å være varierende i de to casene. Det grove meshet overestimerte bruddlasten med 7-12% sammenlignet med det veldig fine meshet i Plaxis 2D, og med 7-20% sammenlignet med det fine meshet i Plaxis 3D. Den relativt store overestimeringen i Plaxis 3D er delvis grunnet den dårlige kvaliteten av de 10-node tetraederelementene som benyttes. For modellering av brede brulandkar med plan tøyning indikerer resultatene at Plaxis 2D bør brukes, og at å bruke et fint mesh vil gi nøyaktige resultater. For smalere brulandkar vil Plaxis 3D være mer relevant, og bruk av medium mesh er anbefalt. Når et medium mesh brukes kan det regnes med en overestimering av bruddlasten på 5 til 10%. Forholdet mellom vegghøyde og horisontal forskyvning ved brudd ble funnet å være omtrent δ_h/H = 3%.

Contents

List of Symbols

The next list describes several symbols that will be later used within the body of the document

α	Inclination of wall
$\bar{E}$	Average stiffness
β	Ground slope
δ	Mobilized interface friction angle
δ_h	Horizontal deformation
γ	Unit weight of soil
γ_m	Material factor
κ_A	Active earth pressure coefficient in total stress analysis
κ_P	Passive earth pressure coefficient in total stress analysis
ω	Rotation of the critical element
ϕ	Friction angle
ϕ'	Internal friction angle
ϕ_{peak}	Peak internal friction angle
ϕ_r	Residual internal friction angle
ψ	Dilatancy angle
ρ	Mobilized friction angle

τ	Mobilized shear stress
τ_A	Shear stress on active side
τ_c	Critical shear strenght
τ_p	Shear stress on passive side
A	Area
a	Attraction
c	Cohesion
c_r	Residual cohesion
c_u	Undrained shear strenght
D_r	Relative density
E	Elastic modulus of soil
E'	Input average stiffness in Plaxis
E_{50}^{ref}	Reference stiffness modulus
E_{50}^{ref}	Stiffness parameter
E_{oed}^{ref}	Reference oedometer stiffness
E_{ur}	Unloading-reloading stiffness
E_{ur}^{ref}	Reference unloading-reloading stiffness
F	Safety factor
f	Degree of mobilization
G_s	Specific gravity of soil
H	Height of wall
K_0	At rest earth pressure coefficent
K_A	Active earth pressure coefficient

K_h Horizontal earth pressure coefficient

K_p Passive earth pressure coefficient

k_{50} Average stiffness

L Length of influence zone

m Index parameter giving amount of stress dependency

N Bearing capacity in general bearing capacity equation

p' Effective mean stress

p'_c Effective preconsolidation stress

P_A Resultant active force

p_A Active earth pressure

P_P Resultant passive force

p_p Passive earth pressure

p_v Vertical stress

p_{ref} Reference stress

r Roughness ratio

R_f Hyperbola cut off parameter

R_{inter} Wall interface angle

R_{max} Maximum roughness ratio

S Lateral wall displacement

s_u Undrained shear strenght

u Deformation

v Poisson's ratio

W Width

K System stiffness matrix

k Element stiffness matrix

$\mathbf{k}^i$ Element stiffness matrix

R Nodal loads

r Nodal displacements

S Element nodal point forces

v Element nodal displacements

Chapter 1

Introduction

1.1 Background

Passive earth pressure plays an important role in a wide range of geotechnical and structural engineering problems, as it resists lateral movement of structures and provides stabilizing forces. Internationally the most widely accepted theories for estimating the lateral earth pressures are the Rankine theory and the Coulomb theory. In Norway Janbu's theory, extending Terzaghi's Log Spiral theory, is most commonly used. The earth pressure theories are based on a set of assumptions concerning the properties of the soil, and these assumptions will always at a certain extent be at variance with reality.

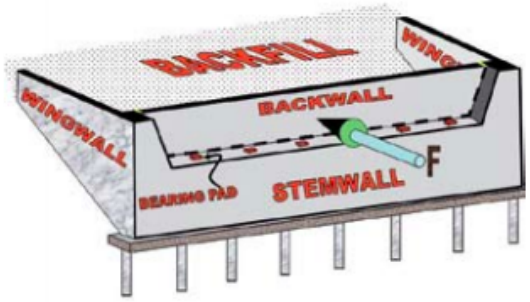

Figure 1.1: Seat type abutment and distribution system (Shamsabadi and Nordal, 2006)

Bridges are subjected to longitudinal forces from stopping traffic, and these forces are normally taken by a passive soil reaction on the bridge abutments (figure 1.1). The passive reaction is mobilized when the lateral displacement increases, resulting in a soil-structure interaction. The bridge usually have bearings in both ends, which will take the vertical forces from the

bridge. The bearings will however allow for a certain horizontal movement, either by slides or by use of rubber bearings that can take a certain lateral strain. If passive earth pressures should provide the resistance against braking forces of traffic, the related deformations of the abutment need to be very limited. Is it possible to achieve a sufficiently high passive earth pressure resistance for limited movements using high quality backfill and proper compaction?

1.1.1 Problem Formulation

The first task is to search for and select a couple of well documented large scale model tests in the literature and to study the set up and the results. Then numerical simulations are to be performed using Finite Element modelling by Plaxis, by both simplified 2D and full 3D models. The soil models and their parameters must be given focus. Parameter calibration should be done by fitting the numerical results to the experimental results. Numerical issues such as artificial overshoot of failure loads due to element types and mesh density should be studied. 2D and 3D simulations should be compared. The simulations, the results and the best fit parameters should be discussed and conclusions drawn.

1.2 Objectives

The main objectives of this thesis are:

- To conduct an extensive literature study on earth pressure and various earth pressure theories.
- To search relevant load tests that are suitable for back-calculations of load-deformation response.
- To back-calculate the load tests using Plaxis 2D and 3D and find suitable input parameters.
- To compare the Plaxis results, hand calculations and results from actual load tests.
- To review the results and give a thorough discussion of the findings.

1.3 Limitations

A number of researchers have proposed various methods for calculation of passive earth pressure. Due to the limited space, only the theories that are most commonly accepted and used are discussed and used for hand calculations in this report.

This study is limited to two load-deformation tests. In order to make more precise conclusions this study would benefit from reviewing additional load tests on gravel backfill, preferably cases where 3D effects are significant.

Only Case 1 is representative for studying the 3D effects on passive resistance of soils. Case 2 consists of a model having 2D geometry that was extruded into a 3D model, and is therefore not appropriate for gaining experience on 3D effects for narrow bridge abutments. Also, numerical issues arose for the two dimensional simulation in Case 2, causing the simulations to stop before reaching failure. Access to the raw data from the reviewed experiments have not been obtained.

Several limitations are connected to the FEM modeling. These models do not give an exact solution to the problem, and provide us only with approximations. The tests have been modeled as closely to the actual test geometry as possible, but several simplifications have been made. Only the Hardening Soil Model has been used for modeling the backfill. Using a different material model could possibly provide more accurate results.

1.4 Approach

Initially a literature study will be performed to obtain a better understanding of earth pressure and several earth pressure theories. To be able to understand the mechanisms in Plaxis, the Finite Element Method and Hardening Soil Model will be studied in depth.

Then two load tests will be reviewed and back-calculated using Plaxis 2D and 3D. The models in Plaxis 2D and 3D will be made to resemble the actual load test setups as closely as possible.

First the models will be run using the material parameters obtained from laboratory tests and calculations. Then the parameters will be adjusted by trial and error to obtain a load-deflection curve matching the measured load-deflection in the tests. Other relevant output such as incremental strains, deformations, normal- and shear stresses will be obtained. In addition to this, hand calculations using several earth pressure theories will be performed.

Finally a comparison of the results will be done in terms of load-deformation behaviour, earth pressures, mesh dependency and 3D effects. The thesis will be concluded with a summary of all the results, conclusion and recommendations for further work.

1.5 Structure of the Report

The remaining part of the thesis is divided into the following five chapters. Chapter 2 is a literature review where the basis of passive earth pressure is reviewed. In addition to this, four different earth pressure theories are presented and compared. Chapter 3 provides a basis for understanding the Plaxis simulations by presenting the Finite Element Method and soil models. Chapters 4 and 5 contain the first and second case study, with Plaxis 2D and 3D results, hand calculations and discussion. A summary of key findings and experiences as well as recommendations for further work are given in chapter 6.

Chapter 2

Literature Review on Earth Pressure

Chapters 2.1 to 2.5 are mainly based on Emdal et al. (2015).

Structural elements in soil will be subjected to earth pressures. Aarhaug (1984) describes earth pressures as normal- and shear stresses acting in the interface of soil and structure. Lateral earth pressure is the pressure the soil exerts in the horizontal direction. The following analyses are most relevant in the case of dimensioning of sheet pile walls and support walls. If we drive a sheet pile wall in the ground and excavate on one side, we will have a situation as shown in figure 2.1. On the excavation side the earth pressure will be significantly reduced. The soil on the other side will push the wall outwards. The wall's movement will determine whether a passive or active state occurs in the soil. To explain these two states a retaining wall will be used, as shown in Emdal et al. (2015), as an example.

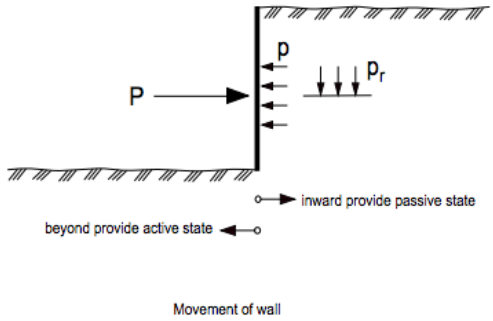

Figure 2.1: Earth pressure - principle sketch (Emdal et al., 2015)

2.1 Passive and Active Earth Pressure

Passive Earth Pressure

In order to push the wall into the soil, the horizontal retaining force needs to increase significantly. A horizontal pressure between the soil and wall occurs. If the force is large enough the soil goes to failure, and a soil wedge will be pushed inwards and upwards as shown in figure 2.2. In this situation the soil is considered to be the *passive* part, and therefore this situation is called a passive stress condition (Emdal et al., 2015).

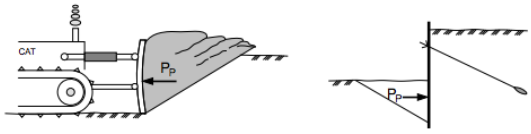

Figure 2.2: Example on passive earth pressure (Emdal et al., 2015)

Active Earth Pressure

The active state occurs when the retaining force acting on the wall is reduced. Reduction of the force leads to the pressure behind the wall being reduced, and an active earth pressure occurs behind the wall. In this case the soil plays the active part in the situation, and the strut force the minor. It is found that only a minor reduction in force will lead to failure in the soil, and a soil wedge will slide down and push the wall outwards as shown in figure 2.3. Active stress situation is found behind all retaining walls that are not braced (Emdal et al., 2015).

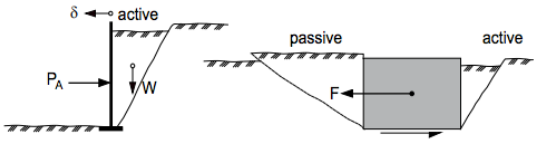

Figure 2.3: Example on active earth pressure (Emdal et al., 2015)

2.2 Total Stress Analysis

The total stress analysis (s_u analysis) uses the undrained strength of the soil, and includes both stress acting on the soil grains and stress due to water. The critical elements in s_u-analysis are

quadratic, meaning $\alpha = 45°$.

In active state the stress conditions become as shown in figure 2.4. The wall is pushed outwards, the horizontal stress p_A decreases and the vertical stress p_v becomes the major principal stress.

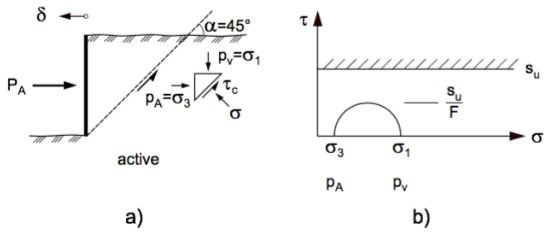

Figure 2.4: Active earth pressure, s_u basis, $r = 0$ (Emdal et al., 2015)

This means that $p_v = \sigma_1$ and $p_A = \sigma_3$. Using Mohr's circle as shown in figure 2.4 the equation for active earth pressure is obtained in equation 2.1:

$$p_A = p_v - 2\frac{s_u}{F} \tag{2.1}$$

In passive state the stress conditions become as shown in figure 2.5.

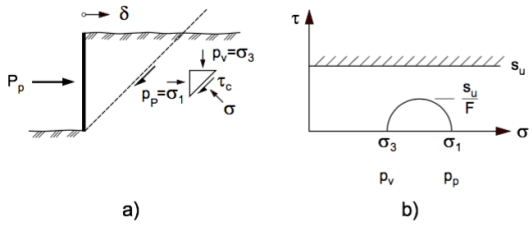

Figure 2.5: Passive earth pressure, s_u basis, $r = 0$ (Emdal et al., 2015)

When the wall is pushed inwards the horizontal stress p_P increases and becomes the major principal stress. Hence $p_v = \sigma_3$. Using the Mohr circle the expression for passive earth pressure is obtained in equation 2.2:

$$p_P = p_v + 2\frac{s_u}{F} \tag{2.2}$$

2.3 Effective Stress Analysis

The critical element in an effective stress analysis is dependent on the friction angle ϕ of the soil. Figure 2.6 displays the rombic shaped critical elements and the stress conditions behind the wall for active and passive state. Note that the smallest element angle is 90° - α and the largest is 90° + α.

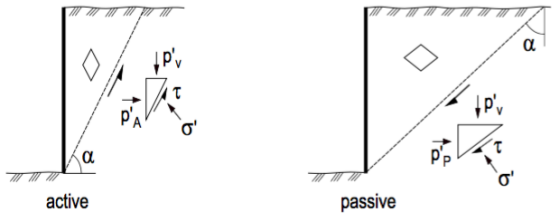

Figure 2.6: Active and passive earth pressure, effective stress analysis, r = 0 (Emdal et al., 2015)

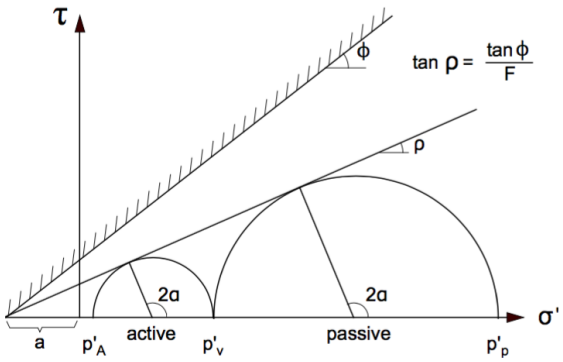

Figure 2.7: Stresses and orientation for active and passive earth pressure on effective stress basis (Emdal et al., 2015)

The effective stress analysis has the same stress relations as in s_u basis: In active state $p'_A = \sigma'_1$ and $p'_v = \sigma'_3$, in passive state $p'_P = \sigma'_3$ and $p'_v = \sigma'_1$. Using the Mohr circle in figure 2.7, expressions for stresses in active and passive state can be derived.

Principal stress ratio:

$$\sigma'_1 + a = N(\sigma'_3 + a), N = \frac{1 + sin\rho}{1 - sin\rho} \tag{2.3}$$

$$\sigma'_3 = \frac{1}{N}(\sigma'_1 + a) - a \tag{2.4}$$

Active state:

$$p'_A = \frac{1}{N}(p'_v + a) - a \tag{2.5}$$

Passive state:

$$p'_P = N(p'_v + a) - a \tag{2.6}$$

2.4 Friction between Soil and Wall

Previously in this chapter the relations for earth pressure on smooth walls (r = 0) are explained. This is however not very realistic, as most walls have a rough surface. In this case shear stresses τ_A and τ_p occur between the wall and soil, and the wall is no longer a principle stress plane. This may lead to the wall being forced to move relatively to the soil movement (Emdal et al., 2015), which is very important to consider when constructing a bridge abutment. Friction between soil and the wall has a significant impact on the size of the earth pressure and the shape of the failure surfaces. Figure 2.8 shows the effect on the failure surface as the roughness ratio r changes.

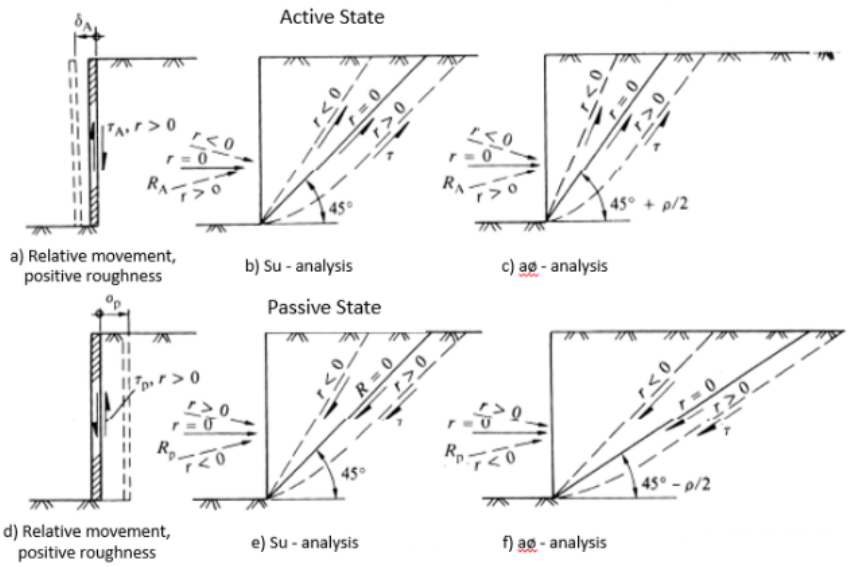

Figure 2.8: Effect of wall roughness in active and passive state (Aarhaug, 1984) (Figure modified to include english captions obtained from Magar (2016))

The roughness ratio r is described as the ratio between mobilized shear stress on the wall τ and the critical shear strength of the soil τ_c, see equation 2.7

$$r = \frac{\tau}{\tau_c} \tag{2.7}$$

If r = 0 the mobilized shear stress on the wall $\tau = 0$. This implies that the wall is completely frictionless, and that no upward or downward forces are transferred from the soil to the wall. In this case the wall becomes a principle stress plane. (Emdal et al., 2015).

Positive and Negative Roughness

In active state, when the wall is pushed outwards (figure 2.8a), the soil will usually slide down behind the wall. This movement creates shear stresses between the wall and soil which then "drags" the wall downwards. This is defined as positive roughness for active state (Aarhaug, 1984).

In passive state the wall is pushed into the soil, and pushes the soil upwards relative to the wall (figure 2.8b). This generates shear stresses which will try to push the wall upwards. This is defined as positive roughness for passive state (Aarhaug, 1984).

In addition to the degree of mobilization $f = 1/F$, the roughness ratio r has the greatest impact on the magnitude of the earth pressure.

2.5 Stress Fields in a-ϕ Analysis

To describe stress fields caused by earth pressure in an idealized case with horizontal terrain and weightless soil, three distinct stress zones or -elements are used (Emdal et al., 2015):
1) The skew element is a rotated Rankine element, where the rotation is caused by a stress component along the wall surface.
2) The Prandtl zone is a stress zone that ties the two outer zones and still maintains equilibrium. Through the Prandtl zone the principal stress directions rotates.
3) The Rankine zone (passive or active) is a Rankine element with major principal stress in horizontal (passive) or vertical (active) direction.

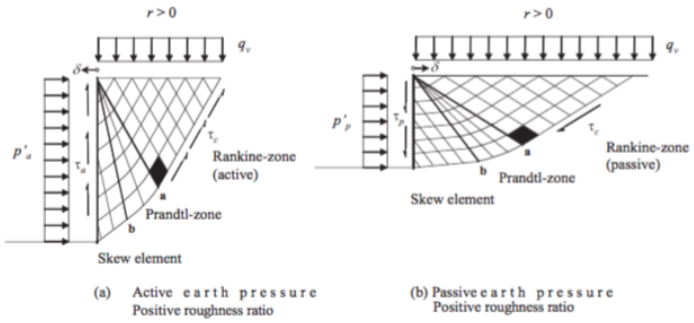

Figure 2.9: Stress fields at earth pressure, $r > 0$ (Emdal et al., 2015)

In figure 2.9 the stress fields for two general cases are displayed. The rotated skew element is the key to understanding the mechanism of the stress fields, and it is dependent on the roughness ratio r. With zero shear stress on the wall the roughness ratio r = 0, which means the opening of the Prandtl zone is zero, and the skew element will have the same opening as the Rankine zone. If the shear stress increases the skew element will start rotating, and the opening angle of the Prandtl zone increases. In the extreme case ($r = 1$) the skew element will be gone, and the Prandtl zone will fill the gap between the Rankine zone and the wall (Emdal et al., 2015).

2.6 Earth Pressure Theories

It is important to note that the theory of lateral earth pressure is not an exact science, and provides us only with a working hypotheses. Several theories have been suggested, and internationally the Coulomb and Rankine theories are widely used, while Janbu's theory is most commonly used in Norway. Experiments have concluded that these theories tend to be inaccurate when compared to the actual passive resistance.

Terzaghi (1943) describes how practically every theory in applied mechanics is based on a set of assumptions concerning the mechanical properties of the materials involved, and how these assumptions always to a certain extent are at variance with reality. Because the behaviour of sands and clays are so complex, mathematical procedures are often too complicated to be utilized in general design of structures, and it is necessary to make simplifying assumptions. This subchapter will explain and compare four earth pressure theories. There are also some differences between the Norwegian and the international approach, which will be explained at the

end of this chapter.

2.6.1 Rankine Theory

The Rankine theory (Rankine, 1857) treats the earth pressure problem in terms of stresses, and assumes a plane failure surface. The theory also assumes no wall friction ($r = 0$), homogeneous soil and that the resultant force acts parallel to the backfill slope. For the passive failure this gives failure surfaces with the angle 45° - $\phi/2$. The passive earth pressure is determined by equation 2.8, where the cohesion often is set to zero.

$$\sigma_p = \sigma_v K_p + 2c\sqrt{K_p} \tag{2.8}$$

The Rankine earth pressure coefficients K_A and K_p are given in equation 2.9:

$$\begin{aligned} K_a &= tan^2(\frac{\pi}{4} - \frac{\phi}{2}) \\ K_p = \frac{1}{K_a} &= tan^2(\frac{\pi}{4} + \frac{\phi}{2}) \end{aligned} \tag{2.9}$$

The only variable in the equations for earth pressure coefficients in Rankine theory is the friction angle ϕ and the cohesion c. The theory does not consider the roughness of the wall, the inclination of the wall or the ground slope. The theory also assumes linear horizontal stress distribution. Note that the Rankine theory is utilized in subchapters 2.1 to 2.3 where $r = 0$.

2.6.2 Coulomb Theory

The Coulomb theory (Coulomb, 1776) treats the problem in terms of forces. This method also assumes a plane failure surface, but it does take into account the value of the wall friction angle δ and the slope of the backfill. The Coulomb passive earth pressure coefficient K_p can be determined numerically using equation 2.10. α is the inclination of the wall in relation to the vertical axis, β is the ground slope, ϕ' is the internal friction angle and δ is the wall friction angle. K_p can also be determined graphically using the chart in figure 2.10. The Coulomb theory is applicable for varying backfill slopes and takes into account the inclination of the wall.

$$K_p = \frac{sin^2(\alpha - \phi')}{sin^2(\alpha) \cdot sin(\alpha + \delta) \cdot (1 + \sqrt{\frac{sin(\phi' + \delta) \cdot sin(\phi' + \beta)}{sin(\alpha + \delta) \cdot sin(\alpha + \beta)}})} \tag{2.10}$$

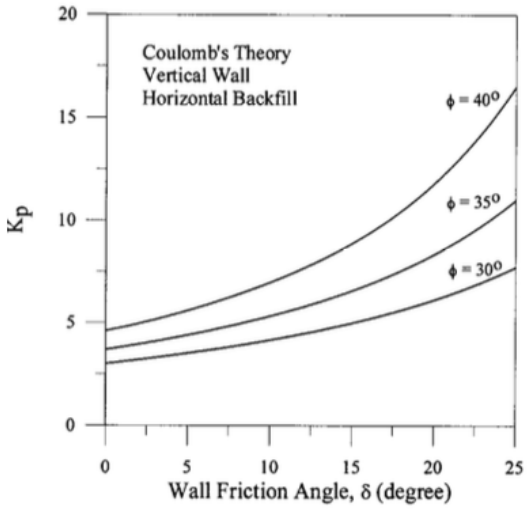

Figure 2.10: Variation of K_p obtained from Coulomb's theory (Coulomb, 1776) (Redrawn by Fang et al. (2002))

2.6.3 Logarithmic Spiral Theory

Terzaghi argued that the assumption of a plane failure surface often grossly overestimates the passive resistance of walls. In contrast to Coulomb and Rankine, Terzaghi (1943) and Terzaghi et al. (1996) indicate that the real failure surface consists of a curved lower part, and a straight upper part, as shown in figure 2.11. The curvature near the wall depends on the wall friction angle δ.

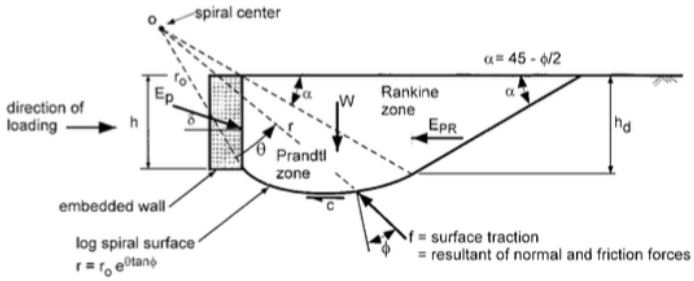

Figure 2.11: Log spiral failure mechanism (Duncan and Mokwa, 2001)

Assuming a curved failure surface makes the model less conservative, as the observed real failure surfaces often tend to be curved. The earth pressure coefficient K_p can be determined numerically using equation 2.11 or graphically using the chart in figure 2.12.

$$K_{p,a} = \frac{1}{cos^2\phi}\left[2cos^2\beta + 2\left(\frac{c}{\gamma z}\right)cos\phi \cdot sin\phi \pm\left\{4cos^2\beta(cos^2\beta - cos^2\phi) + 4\left(\frac{c}{\gamma z}\right)^2 cos^2\phi + 8\left(\frac{c}{\gamma z}\right)cos^2\beta \cdot sin\phi cos\phi)\right\}^{0,5}\right] - 1 \tag{2.11}$$

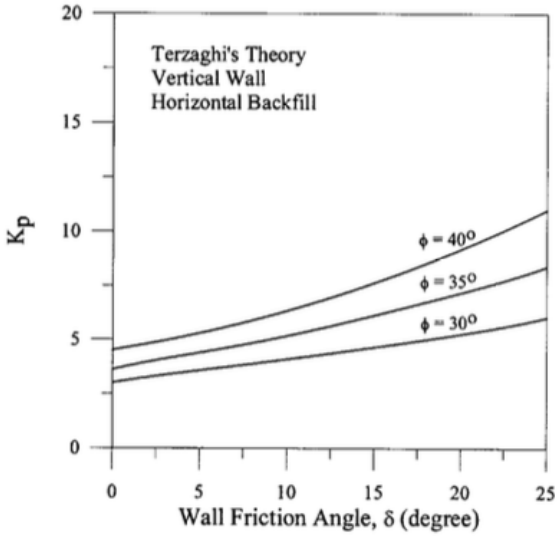

Figure 2.12: Variation of K_p obtained from Terzaghi's Log Spiral theory (Terzaghi et al., 1996) (Redrawn by Fang et al. (2002))

2.6.4 Janbu Theory

Janbu's theory of earth pressure (Janbu, 1972) stands out from the others due to the use of the roughness ratio parameter r and the mobilized friction angle ρ. Like Terzaghi, Janbu's theory also assumes a partially curved failure surface. The earth pressure coefficients can be determined graphically using the chart in figure 2.13 or numerically using equations 2.12 and 2.13.

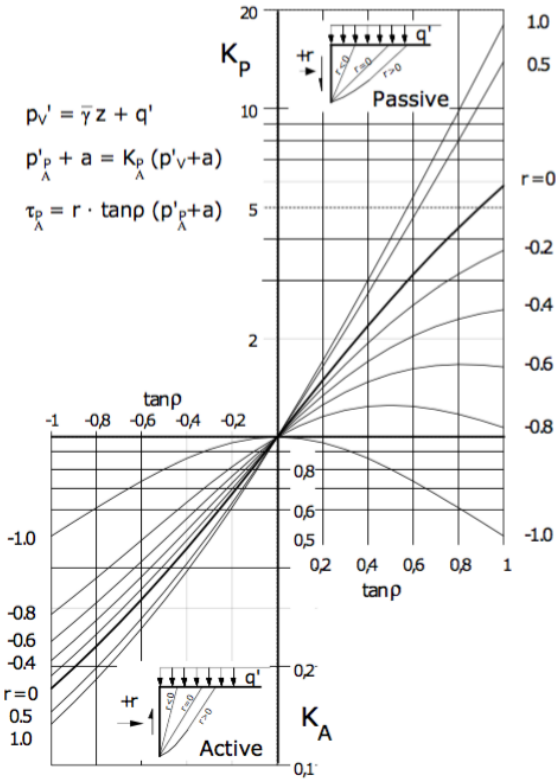

Figure 2.13: Janbu's earth pressure coefficients for effective stress analysis (Emdal et al., 2015)

$$K_P = \left(\frac{1}{\sqrt{1 + tan^2\rho} - tan\rho \cdot \sqrt{1 + r}} \right)^2 \tag{2.12}$$

$$K_A = \frac{1}{K_P} \tag{2.13}$$

2.6.5 Advantages and Limitations

Table 2.1 (Duncan and Mokwa, 2001) describes the advantages and limitations of the Rankine, Coulomb and Log Spiral theories. In addition to this it should be noted that the four theories

mentioned do not directly include the dilatancy angle ψ. However, the dilatancy angle is implicitly included by assuming $\psi = \phi$ (Kowalska, 2015). When gravel is compacted the dilatancy angle may change, which may have an impact on the resulting passive earth pressure. Also, the theories assume linear horizontal stress distribution, which is not always the case (Matsuzava and Hazarika, 1996). The effects of how much the wall moves are not accounted for (Rhodes, 2001).

Table 2.1: Advantages and limitations of some passive earth pressure theories (Modified by author to include roughness ratio r) (Duncan and Mokwa, 2001)

Theory	Advantages	Limitations
Rankine	• Simplest method	•Assumes r=0 •Applies only to simple conditions (planar ground surface, uniform surcharge, homogeneous soil)
Coulomb	• Applicable for any value of r and δ • Easy to apply through charts, tables or formulas • Can account for more complex conditions (irregular ground surface, nonuniform surcharge, nonhomogenous soil conditions) through graphical analysis	• Passive pressures are too high for values of δ >0,4ϕ • Complex conditions require graphical analysis
Log spiral charts and tables	• Accurate for any value of r and δ • Easy to apply	• Applicable only to simple conditions • Does not accommodate cohesive component of shear strenght
Log spiral graphical solution	• Accurate for any value of r and δ • Can accommodate cohesive as well as frictional strenght • Is applicable to complex conditions	• Requires complex graphical analysis
Log spiral numerical solution	• Accurate for any value of r • Can accommodate cohesive as well as frictional strength • With Ovesen's correction: Accounts for 3D effects	• Computer program such as PYCAP is needed • PYCAP is only applicable to simple conditions (level ground, vertical wall, uniform surcharge and homogenous soil)

2.6.6 Roughness Ratio r versus Wall Friction Angle δ

In Norway Janbu's method of determining earth pressure coefficients is commonly used. This method uses the values of roughness ratio r and mobilized friction angle ρ to determine the coefficients. This approach differs from the international method which uses the relation between wall friction angle δ and friction angle ϕ to determine coefficients. In order to be able to understand the results obtained in international experiments, it is necessary to understand the correlation between r, ρ, δ and ϕ.

As explained in chapter 2.4, the roughness ratio r is the ratio between the mobilized shear stress on the wall τ_v and the critical shear strength of the soil τ_c. The maximum allowed mobilized friction angle ρ is dependent on the material factor γ_M which usually is between 1,25 and 1,40 (equation 2.14 and figure 2.14).

$$tan\rho_{max} = \frac{tan\phi}{\gamma_M} = f_{max} \cdot tan\phi \tag{2.14}$$

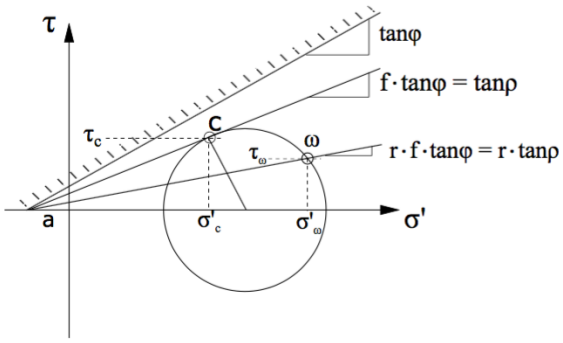

Figure 2.14: Mohr-Coulomb failure criterion (Emdal et al., 2015)

Figure 2.14 gives the equation for τ_v, valid for any r and any degree of mobilization:

$$\tau_v = r \cdot tan\rho(p'_h + a) \tag{2.15}$$

which can be rewritten:

$$\tau_v = r \cdot f \cdot tan\phi(p'_h + a) \tag{2.16}$$

Hence the ultimate maximum shear stress τ_{max}, assuming fully mobilized soil ($f = 1$) and

denoting the maximum roughness ratio r as R_{max} will be:

$$\tau_{max} = R_{max} \cdot tan\phi(p'_h + a) \tag{2.17}$$

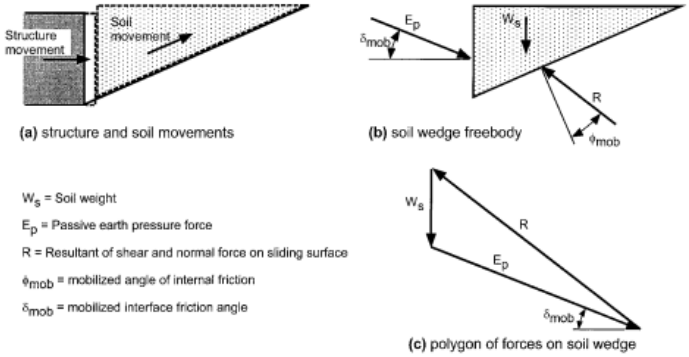

Figure 2.15: Movements, forces and equilibrium requirements for passive pressure conditions (Duncan and Mokwa, 2001)

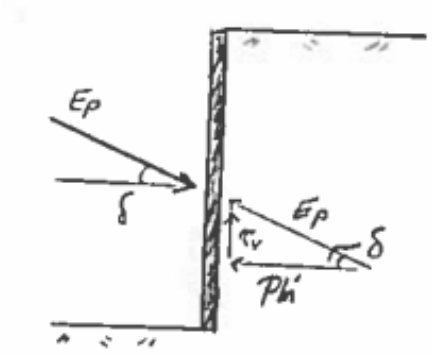

Figure 2.16: Resultant force E_p acting on the wall

The international approach uses the parameter wall friction angle δ. The use of this parameter is varying. Sometimes a mobilized wall friction angle δ_{mob} is used, assuming the soil is partially mobilized. Other times the ultimate value δ_{peak} is used, assuming fully mobilized soil. Using figures 2.15 and 2.16 the equation for shear stress on the wall is found to be:

$$\tau_v = tan\delta(p'_h + a) \tag{2.18}$$

Combining equation 2.17 and 2.18 gives:

$$tan\delta_{peak} = R_{max} tan\phi \tag{2.19}$$

This means that for the ultimate limit state the correlation between $r = R_{max}$ and δ_{peak} is:

$$R_{max} = \frac{tan\delta_{peak}}{tan\phi} \tag{2.20}$$

For partially mobilized soil, combining equations 2.16 and 2.18 gives:

$$tan\delta_{mob} = r \cdot f \cdot tan\phi \tag{2.21}$$

Giving a correlation between r and δ_{mob}:

$$r = \frac{tan\delta_{mob}}{f \cdot tan\phi} \tag{2.22}$$

Chapter 3

Calculation Methods

3.1 Finite Element Method (FEM)

The finite element method is a numerical calculation method, and the term finite element was first used by Ray W. Clough in 1956 (Clough et al., 1956). Due to its versatility and high computational efficiency, finite element analysis is dominating the engineering analysis software market. In FEM the structure is divided into a set of elements interconnected in discreete points called nodes, as displayed in figure 3.1 (Bell, 2013).

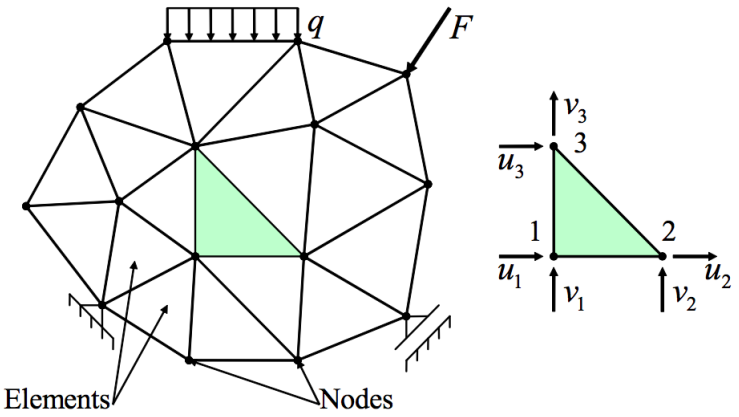

Figure 3.1: A plane stress region divided into triangular elements (Mathisen, 2017)

The mathematical model with an infinite number of degrees of freedom (DOFS) is approximated with a discrete model with a finite number of DOFS. For each element displacement is described in terms of nodal shape functions that determine the form of the displacement field in the element (Mathisen, 2017). To be able to interconnect elements in a system, the relation

between the nodal forces and the nodal point displacements must be obtained. The element stiffness relationship is given in equation 3.1,

$$\mathbf{S} = \mathbf{kv} \tag{3.1}$$

where **S** is the element nodal point forces, **k** is the element stiffness matrix and **v** is the element nodal displacements. The relationship between nodal loads **R** and nodal displacements **r** is shown in equation 3.2.

$$\mathbf{R} = \sum_{i=1}^{m} \mathbf{g}^i \mathbf{S}^i = \sum_{i=1}^{m} \mathbf{g}^i \mathbf{k}^i \mathbf{v}^i = (\sum_{i=1}^{m} \mathbf{g}^i \mathbf{k}^i \mathbf{a}^i)\mathbf{r} = \mathbf{Kr} \tag{3.2}$$

Where i is the element number and m is the total number of elements in the system. The term $\mathbf{g}^i\mathbf{S}^i$ is an expression for the forces that element number i exerts on all nodal points. $\mathbf{k}^i$ is the element stiffness matrix, and **K** is the system stiffness matrix Bell (2013).

According to Bell (2013) the process of finite element analysis requires three basic steps:

1. **Preprocessing Phase.** Create and discretize the the problem into finite elements. This involves choosing an appropriate element type, creating a FE mesh with proper mesh density and discretizing the representation of loads and boundary conditions.

2. **Solution Phase.** Solve a set of linear algebraic equations to obtain nodal results.

3. **Postprocessing Phase.** Compute strains and stresses from nodal results, access the accuracy of the FE solution.

Like in other calculation methods, errors can contaminate the results of a finite element analysis. The errors introduced during the process of finite element analysis are classified into three main categories. *Modelling errors* (also called idealization errors) are caused by the modification of the CAD-model; *discretization errors* are due to the discretization of the mathematical model and *numerical errors* are caused by the accumulation of round-off errors (Mathisen, 2017).

3.2 Plaxis 2D

Plaxis 2D is a finite element program intended for two-dimensional analysis of stability and deformation in geotechnical engineering and rock mechanics. The program is used to perform stability, deformation and flow analysis for various types of geotechnical applications. Real situations may be modelled either by a plane strain or an axisymmetric model (Plaxis, 2018). In Plaxis 2D the 15-node triangles as displayed in figure 3.2 are the most commonly used option for the basis of soil elements. The element has two DOFS per node: u_x and u_y. The 15-noded triangles provide a fourth order interpolation for displacements.

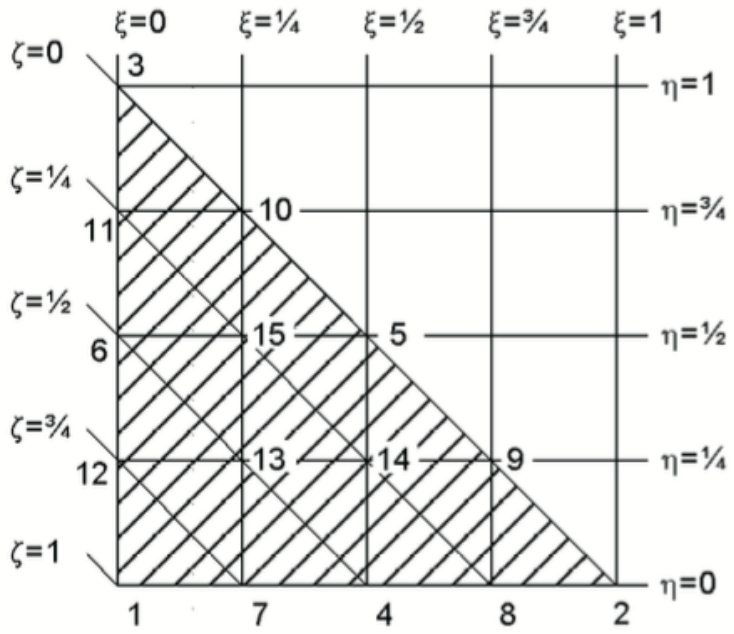

Figure 3.2: Local numbering an positioning of nodes of a 15-node triangular element (Plaxis, 2018)

Like other finite element programs the calculation method is not exact. The error may however be reduced by applying a finer mesh. Eight different material models can be used in Plaxis 2D, with various degrees of accuracy:

- Linear Elastic model (LE).
- Mohr-Coulomb model (MC)
- Hardening Soil model (HS)
- Hardening Soil model with small-strain stiffness (HSsmall)

- Soft Soil model (SS)
- Soft Soil Creep model (SSC)
- Jointed Rock model (JR)
- Modified Cam-Clay model (MCC)

The Linear Elastic model is based on Hooke's law of isotropic elasticity, and may be used to model stiff volumes in the soil, like concrete walls. The Mohr-Coulomb model is often used for a first analysis of the problem considered, because of the short simulation time. Mohr-Coulomb model includes five parameters: E and ν for soil elasticity and ϕ, c and ψ for soil plasticity. (Plaxis, 2018). The Hardening Soil model is a more advanced model with higher accuracy, and will be further described in section 3.5.

3.3 Plaxis 3D

Plaxis 3D is a finite element program used for three-dimensional analysis. The 10-node tetrahedral elements as displayed in figure 3.3 are used for the basis of soil elements in Plaxis 3D. The tetrahedal element has three DOFS per node: u_x, u_y and u_z (Plaxis, 2017). This element provides a second order interpolation for displacement.

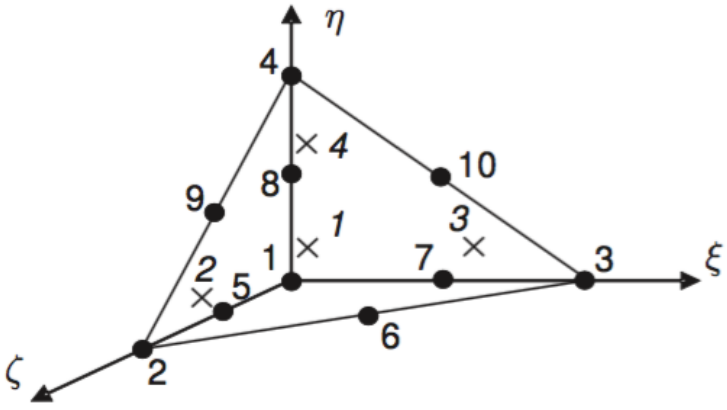

Figure 3.3: Local numbering an positioning of nodes of a 10-node triangular element (Plaxis, 2018)

Plaxis 3D offers the same eight material models as Plaxis 2D. For cases where 3D effects are significant Plaxis 3D is expected to provide more accurate calculations than Plaxis 2D. However,

a three dimensional simulation requires longer execution- and computation time, and is therefore more expensive.

3.4 Mohr-Coulomb Model

The Linear-Elastic Perfectly-Plastic Mohr-Coulomb model involves five input parameters: Young's modulus E and Poisson's ratio ν for soil elasticity, cohesion c, friction angle ϕ and dilatancy angle ψ for soil plasticity (Plaxis, 2018). When using this model an average constant stiffness is used, which makes it possible to perform simpler calculations.

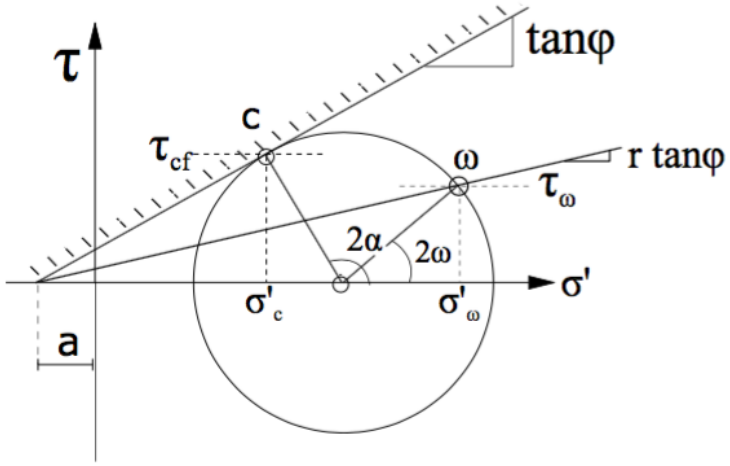

Figure 3.4: The Mohr-Coulomb failure criterion (Emdal et al., 2015)

The Mohr-Coulomb criterion is illustrated in figure 3.4. A failure envelope is determined by the friction angle and cohesion (Coulomb criterion), and the stresses are illustrated by Mohr's circle (Emdal et al., 2015).

3.5 Hardening Soil Model

The Hardening Soil model is an advanced soil model commonly used in Plaxis. The model was originally proposed for sand, but is now further developed to be used also for other soil types. The original Hardening Soil model was developed by Schanz (1998) and Vermeer et al. (1999).

The Hardening Soil model is an elasto-plastic model with hardening connected to two plas-

tic yield surfaces. The first yield surface is a "cone", described by the Coulomb-criterion with the mobilized friction $tan\rho$. When loading towards failure the cone will gradually expand and give plastic strains controlled by the increase in mobilized friction (Nordal, 2017).

The second surface is the so-called "cap" or spherical surface. Its position is controlled by the preconsolidation stress p'_c. When loading below the "cap" the soil is still in the preconsolidated area, but with increasing p' the "cap" will be reached. When loading further with increasing p' the soil behaviour changes, the "cap" expands, and plastic volumetric strains develop as a consequence (Nordal, 2017).

The Hardening Soil Model, like the Mohr-Coulomb, describes the stress levels in terms of friction angle ϕ, cohesion c, and dilatancy angle ψ. In addition to this, several stiffness parameters are brought in, controlling loading in shear, volumetric loading and unloading. Plaxis defines the stiffness using three independent stiffness parameters: stiffness for deviatoric loading, E_{50}, the unloading stiffness, E_{ur}, and the oedometer stiffness, E_{oed}.

The stress-strain behaviour for primary loading is non-linear. For small strain the parameter E_{50} is used instead of the initial modulus E_i. It is given by equation 3.3 (Vermeer et al., 1999).

$$E_{50} = E_{50}^{ref} \left(\frac{\sigma'_3 + a}{p_{ref} + a} \right)^m \tag{3.3}$$

E_{50}^{ref} is a reference stiffness modulus corresponding to the refrence stress p^{ref}, and is a Plaxis input parameter. The actual stiffness, E_{50}, is dependent on the minor principal stress, σ'_3, which is the confining pressure in a triaxial test. The index m gives the amount of stress dependency of the soil. The modulus E_{50}^{ref} is determined by examining the triaxial stress-strain curve for a 50 percent mobilization of the maxiumum shear strenght q_f, see figure 3.5 (Vermeer et al., 1999).

For unloading and reloading the modulus E_{ur} is used, with E_{ur}^{ref} as the reference Young's modulus for unloading and reloading, see equation 3.4.

$$E_{ur} = E_{ur}^{ref} \left(\frac{\sigma'_3 + a}{p_{ref} + a} \right)^m \tag{3.4}$$

The unloading-reloading path is modeled as purely non-linear elastic (Vermeer et al., 1999). The poisson's ratio ν_{ur} for un-/reloading has a low value, usually in the range 0,1 to 0,2. During loading plastic strains occur, making loading softer than unloading (Nordal, 2017). E^{ur}_{ref} is therefore often set to $3E^{50}_{ref}$, which is the default Plaxis value.

In the normal consolidated region the stiffness is given by the parameter E^{oed}_{ref}, see equation 3.5. This modulus is also known as the tangent stiffness for primary oedometer loading. E_{oed} is dependent on σ'_1.

$$E_{oed} = E^{ref}_{oed}\left(\frac{\sigma'_1 + a}{p_{ref} + a}\right)^m \tag{3.5}$$

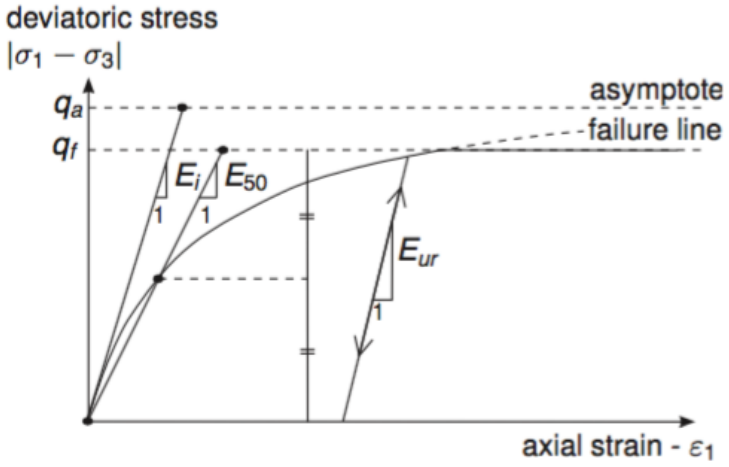

Figure 3.5: Hyperbolic stress-strain relation in primary loading for a standard drained triaxial test (Plaxis, 2018)

Unlike the Mohr-Coulomb, the Hardening Soil Model takes into account the increase of stiffness with increasing stress. Figure 3.6 displays the shear hardening and cap yield surfaces in the Hardening Soil model.

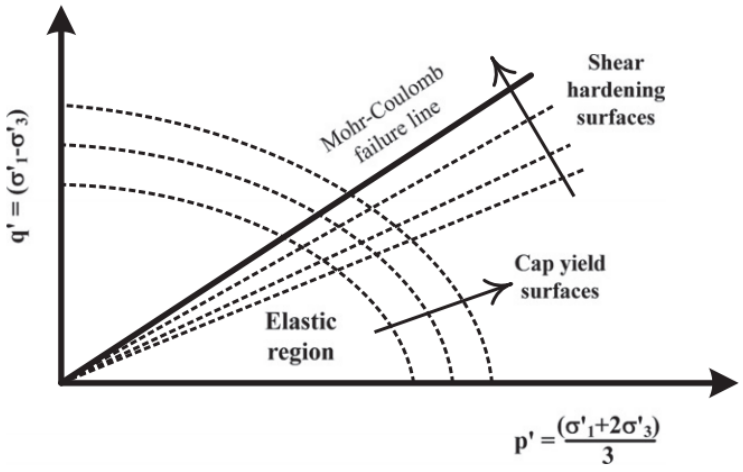

Figure 3.6: Shear hardening and cap yield surfaces in the Hardening Soil model (Vermeer et al., 1999)

Chapter 4

Case 1: Duncan and Mokwa (2001)

4.1 Test Procedure

The passive pressure load tests (Duncan and Mokwa, 2001) were performed at the Virginia Polytechnic Institute (Virginia Tech) field test site at Kentland Farms near Blacksburg, Virginia. The test arrangement is shown in figure 4.1. A pile group was used for reaction, and horizontal loads were applied to a reinforced concrete anchor block. Two tests were performed until failure, one with the anchor block bearing against natural ground and one against compacted gravel backfill (figure 4.2). The anchor block was 1,1 meters high, 1,9 meters long and 0,9 meters thick (3.5 6.3 3.0 ft).

The first test was performed with the anchor block bearing against the natural ground. The anchor block was loaded incrementally, up to a maximum load of 614 kN. This load was maintained for about 90 minutes, while continual deformation occured. After deflections reached 41 mm, the soil in front of the wall failed. A scarp was observed about 1,8 meters in front of the anchor block.

Before the second test, the natural soil was excavated in front of the anchor block to a depth of 1.1 meters and for a distance of 2,3 meters in front of the block. The excavation was filled with gravel backfill, compacted in layers. The anchor block was loaded incrementally, up to a maximum load of 408 kN and maximum deflection of about 38 mm. A disctinct bulge developed at the surface of the backfill 2,3 meters from the front of the anchor block.

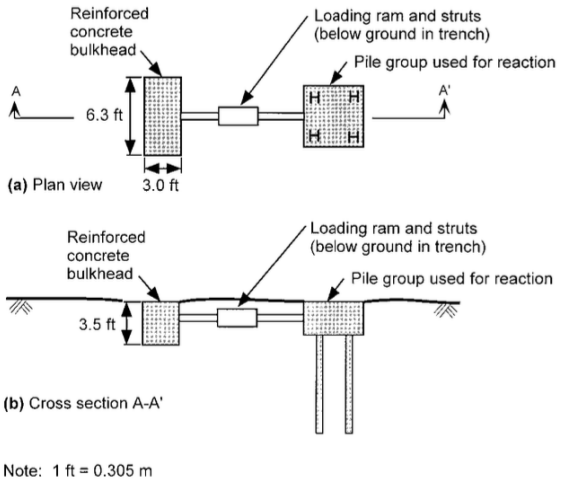

Figure 4.1: Test arrangement for passive pressure load tests (Duncan and Mokwa, 2001)

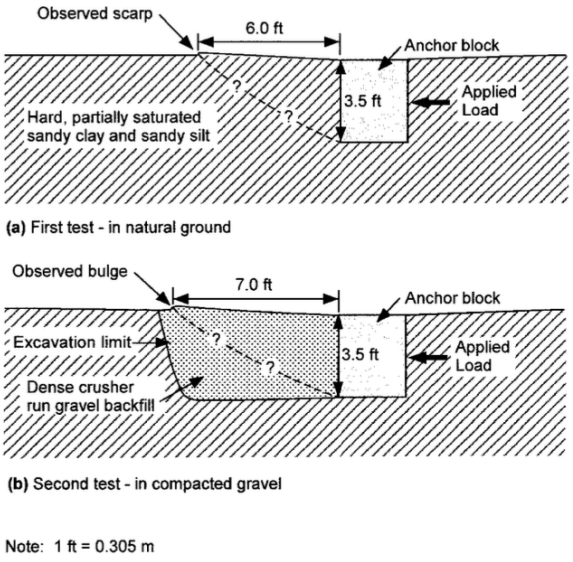

Figure 4.2: Positions of scarp and surface bulge in passive pressure load tests in natural ground and crusher run gravel (Duncan and Mokwa, 2001)

4.2 Soil Properties

The natural soil was found to be hard sandy silt and sandy clay. The measured properties of the material in the field test site are displayed in table 4.1. The parameters were determined by performing unconsolidated-undrained triaxial tests on specimens trimmed from hand-excavated block samples. The samples were taken from above the water table and were only partly saturated, and therefore exibits a large friction angle and cohesion. Undrained conditions are assumed.

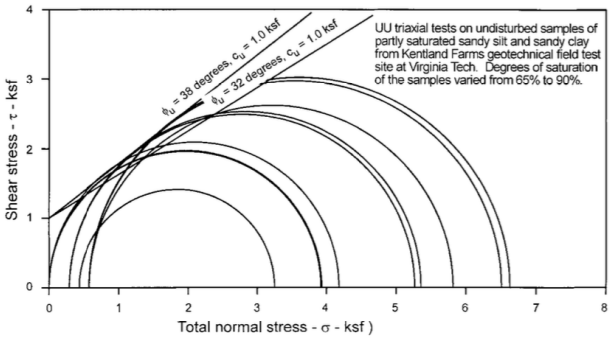

Figure 4.3: Unconsolidated undrained test on natural soil. Note: 1 ksf = 47,9 kPa (Duncan and Mokwa, 2001)

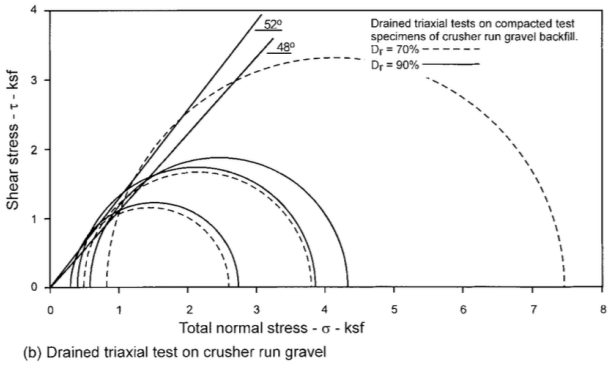

Figure 4.4: Drained triaxial test on crusher run gravel. Note: 1 ksf = 47,9 kPa (Duncan and Mokwa, 2001)

The crusher run gravel backfill in the second test was compacted in layers to a relative density of 80 percent. Test specimens were carefully compacted in the laboratory to the average density measured in the field, and drained triaxial tests were performed. The soil properties suggested by the researchers are displayed in table 4.1. Note that the c for the natural soil is the undrained shear strenght, c_u.

Table 4.1: Soil properties

Soil		$c[kPa]$	$\phi[°]$	$\gamma\ [kN/m^3]$	$E[MPa]$	$v[-](estimated)$
Natural soil	*High*	47,9	38	19,154	47,90	0,33
	Low	47,9	32	21,195	33,53	0,33
Gravel backfill	*High*	0	52	21,195	40,72	0,30
	Low	0	48	21,195	27,78	0,30

4.3 Computation of Stiffness Parameters

In the Hardening Soil model, the applied stiffness for the soil follows the expression in equation 4.1, as explained in section 4.5.

$$E_{50} = E_{50}^{ref} \left(\frac{\sigma_3' + a}{p_{ref} + a} \right)^m \tag{4.1}$$

Assuming a wall of height H is subjected to a horizontal deformation δ_h due to an average horizontal strain within an influence zone L. L is set to a value of $2H$, and k_{50} is the average stiffness for the material. According to Shamsabadi and Nordal (2006) an average stiffness $\bar{E}$ may be introduced by the following equation:

$$\delta_h = \frac{\sigma_h}{\bar{E}} L = \frac{\sigma_h}{\bar{E}} 2H = \frac{P_p}{A\bar{E}} 2H = \frac{P_p}{WH\bar{E}} 2H = \frac{P_p}{W\bar{E}} 2 = \frac{2k_{50}\delta_h}{W\bar{E}} \tag{4.2}$$

Here P_p is 50 % of the ultimate passive earth pressure acting over a total wall area of $A = W \cdot H$. The horizontal stress acting on the wall is $\sigma_h' = P_p / A$. The fraction 50 % is chosen to give a "half-way to failure" average stiffness. In the experiment the wall width is $W = 1,9m$. The average stiffness k_{50} is found from observating the obtained force-displacement relationship of the soil, as shown in equation 4.3.

$$k_{50} = \frac{q_{50}}{u_{50}} \tag{4.3}$$

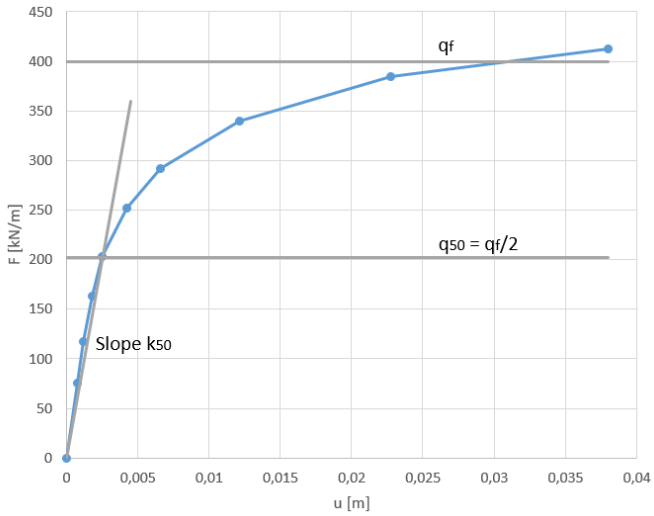

Figure 4.5: Force-displacement relationship gravel and natural soil

The force-displacement curve for natural soil with gravel backfill is given in figure 4.5. This curve correlates to the complex interaction of the two materials, and it is therefore not possible to interpret the material parameters for gravel and natural soil separately. An approximation will be done by assuming that the curve in figure 4.5 is obtained from backfill of gravel only. The force-displacement curve gives the following k_{50} for natural soil with gravel backfill:

$$k_{50} = \frac{q_{50}}{u_{50}} = \frac{200kN}{2,5mm} = 80kN/mm \tag{4.4}$$

From equation 4.4 an expression for the average stiffness is obtained:

$$\bar{E} = \frac{2k_{50}}{W} = \frac{2 \cdot 80kN/mm}{1900mm} = 84MPa \tag{4.5}$$

The gravel is compacted, which may result in an apparent attraction in the material. A cohesion $c = 12kPa$ is assumed, resulting in an attraction $a = 10kPa$. Compaction will also result in an increase of the earth pressure coefficient K_0', which is assumed to be 1,5. The index m is set to 0,5. E_{50}^{ref} is estimated using equation 4.6:

$$E_{50}^{ref} = \bar{E}_{50}\left(\frac{p'_{ref}+a}{\sigma'_3+a}\right)^{1-m} = 84MPa\left(\frac{100kPa+10}{1,5\cdot 11,7kPa+10}\right)^{0,5} = 167MPa \tag{4.6}$$

The load-deflection curves in figures 4.11 and 4.12 indicate that the combination of natural soil and gravel backfill gives larger displacements than that of only the natural soil. It is therefore assumed that the stiffness of the natural soil is greater than the stiffness of the gravel, and the computed value in equation 4.6 is too high. Hence an approximate value of E_{50}^{ref} = 100 MPa is chosen for the gravel backfill. For sand and gravel E_{50}^{ref} is normally within the range of 15 to 50 MPa, but because the backfill material is well compacted a high stiffness is justified (Shamsabadi and Nordal, 2006).

4.4 Plaxis 2D Simulation of Load-Deflection Response

4.4.1 Configuration of Plaxis Model and Boundary Conditions

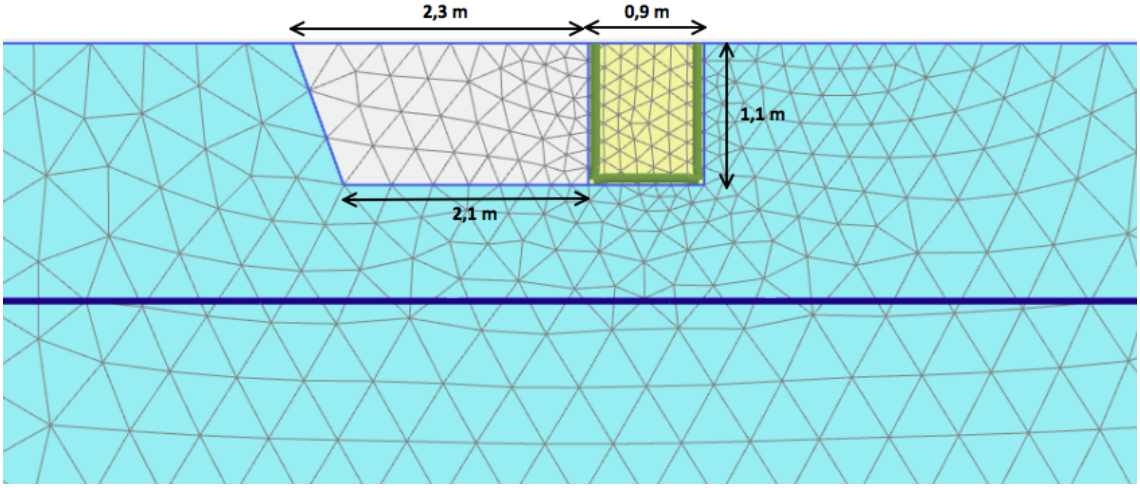

Figure 4.6: Plaxis model

A plane strain FE model was calibrated based on the load test and lab data from the experiment. The boundary conditions and dimensions of the FE model were set to match the test configuration (figure 4.6). The model was 13 meters wide ($x_{min} = 0, x_{max} = 13m$) and 4 meters high ($y_{min} = -4m, y_{max} = 0$). The concrete block had dimensions $0,9m$ x $1,1m$. The gravel backfill was modeled to depth 1,1 meters and distance 2,3 meters in front of the block. The groundwater

table was set to depth 2 meters as the soil samples were taken above the water table. Interfaces were created along the concrete wall to account for the soil-structure interaction. A prescribed uniform horizontal displacement of 4 cm acted along the wall. For the first test the grey soil polygon consisted of natural soil, and for the second test it consisted of gravel. The Mohr-Coulomb and Hardening Soil model was used for modeling the natural soil and gravel backfill, respectively. Plaxis 2D Version 2016.01 was used.

4.4.2 Elements and Mesh

Triangular 15-node elements were used to model the gravel, natural soil and the concrete block. The main simulations were run using a fine mesh. Simulations with coarse, medium and very fine meshes were also performed.

4.4.3 Input Parameters to Finite Element Studies

Table 4.2: Input parameters for modeling of natural soil

Soil	γ $[kN/m^3]$	c [kPa]	ϕ	E' [MPa]	E_{oed} [MPa]	E_{ur}^{ref} [MPa]	m	ψ	ν	R_{int}	R_f	K_0
Natural soil	20	47	0	35	-	-	-	-	0,3	0,75	0,9	automatic
Concrete	23,4	-	-	30 000	-	-	-	-	0,3	0,75	-	-

Table 4.3: Input parameters for modeling of gravel and natural soil

Soil	γ $[kN/m^3]$	c [kPa]	ϕ	E'/E_{50}^{ref} $[MPa]$	E_{oed} $[MPa]$	E_{ur}^{ref} $[MPa]$	m	ψ	ν/ν_{ur}	R_{int}	R_f	K_0 [kPa]
Natural soil	20	35	0	35	-	-	-	-	0,3	0,75	0,9	automatic
Gravel backfill	21,2	0,01	35°	100	100	300	0,5	10	0,2	0,75	0,9	1,5
Concrete	23,4	-	-	30000	-	-	-	-	0,3	0,75	-	-

When modeling the natural soil only, the parameters in table 4.2 were used. To obtain a good approximation the stiffness parameter E' was reduced from 47,9 MPa to 35 MPa. The material parameters in table 4.3 were used for modeling natural soil with gravel backfill. The c_u for natural soil was reduced from 47 kPa to 35 kPa, and E' was set to 35 MPa. For the gravel the friction angle was reduced from 50° to 35°. Undrained conditions were assumed for the natural soil,

and drained for the gravel backfill. The concrete block was modeled with very high stiffness E in order to act rigid.

4.4.4 Computed Results

Deformed Mesh and Incremental Strains

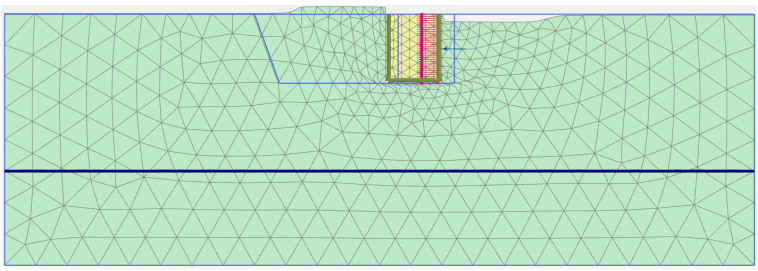

Figure 4.7: Deformed mesh for natural soil

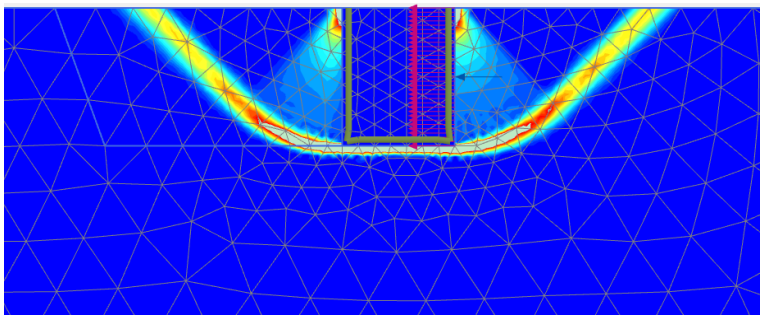

Figure 4.8: Incremental strains for natural soil, fine mesh

Figure 4.7 shows the deformed mesh for load test against natural soil. A bulge is observed at distance 1,8 meters in front of the anchor block. The incremental strains are given in figure 4.8. A Rankine zone and rotated skew element is observed at both sides of the concrete block.

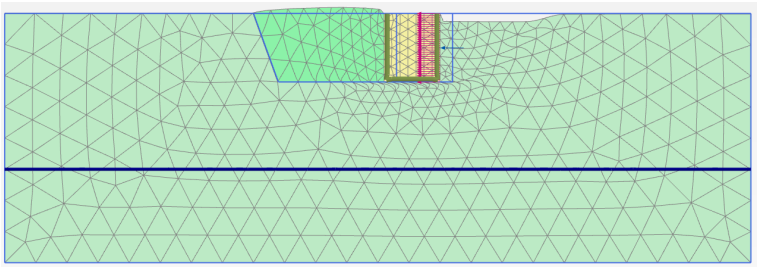

Figure 4.9: Deformed mesh for gravel backfill and natural soil

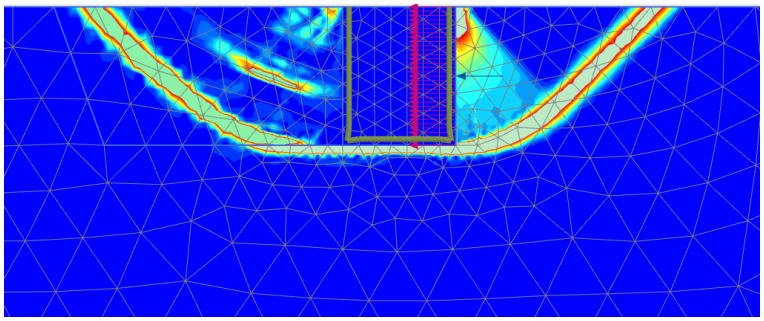

Figure 4.10: Incremental strains for gravel backfill and natural soil, fine mesh

The deformed mesh in figure 4.9 shows a bulge at the surface of the gravel backfill at distance 2,3 meters from the front of the anchor block. Figure 4.10 shows the incremental strains for natural soil with gravel backfill. On the right side of the anchor block the outline of an active Rankine zone and a rotated skew element is observed. A rotated skew element, a Prandlt zone and a passive Rankine zone is observed at the left side. Also, an other failure plane is starting to appear.

Load-Deflection Curves

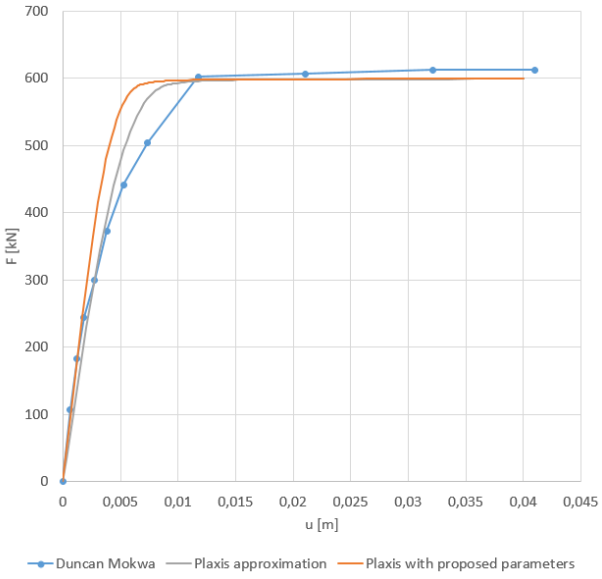

Figure 4.11: Load-deflection curve for natural soil

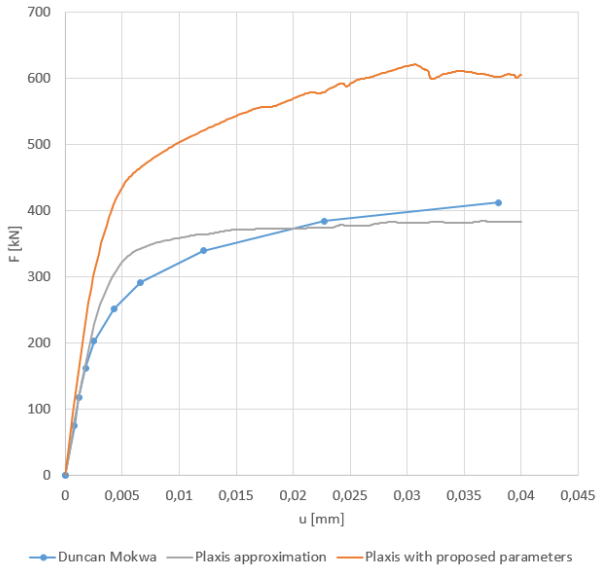

Figure 4.12: Load-deflection curve for natural soil with gravel backfill

The simulated load deflection curves for natural soil are displayed in figure 4.11. Using the material parameters obtained from laboratory tests and calculations (Plaxis with proposed param-

eters curve), the curve is a good fit concerning the measured failure load. By reducing the stiffness E' the steepness of the curve was reduced, and an acceptable approximation was made.

For simulations of natural soil with gravel backfill the load-deflection curves are displayed in figure 4.12. Using the material parameters obtained from laboratory tests and calculations, the simulated load-deflection curve gives a failure load 50% higher than the measured failure load. Using the adjusted parameters in table 4.3 a good approximation was made.

Mesh Dependency

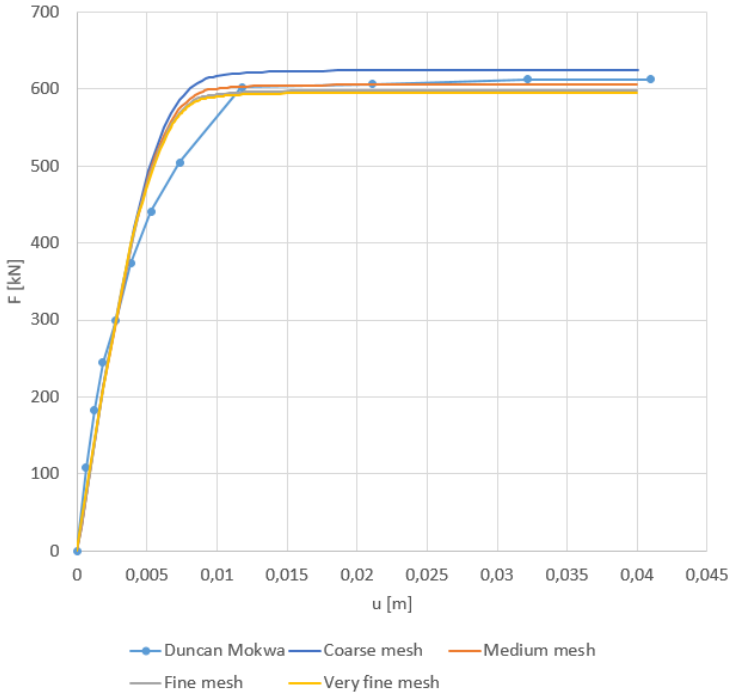

Figure 4.13: Mesh dependency for natural soil in Plaxis 2D

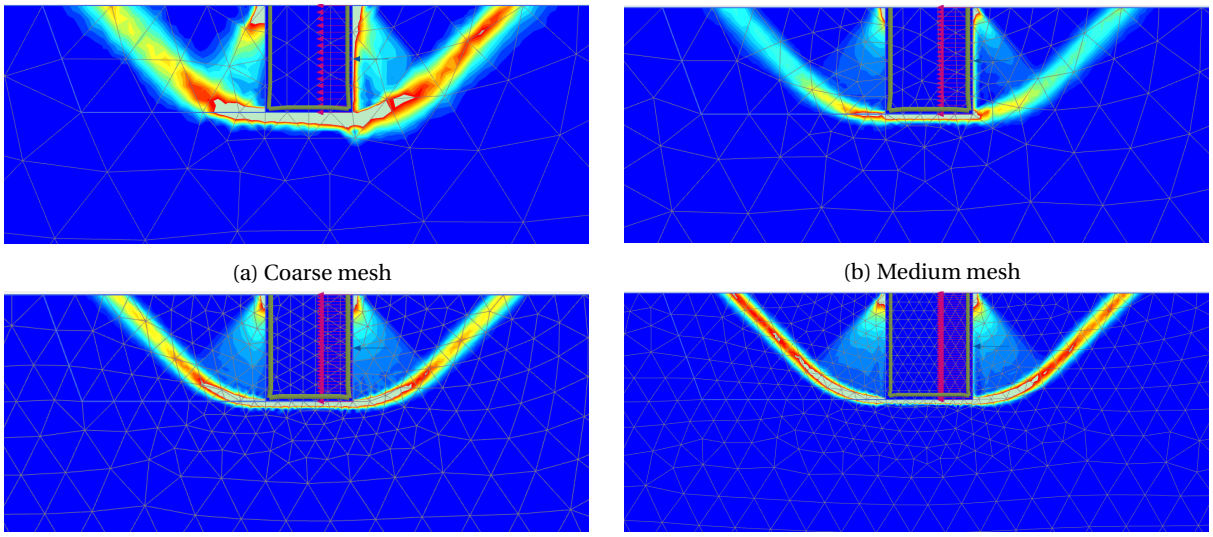

(a) Coarse mesh

(b) Medium mesh

(c) Fine mesh

(d) Very fine mesh

Figure 4.14: Incremental strains for natural soil

The load deflection curves for the natural soil in figure 4.13 are identical up to about 80 % of the failure load, where they start to deviate. The curves for fine and very fine mesh are very similar. The coarse mesh curve displays 5% overshoot compared to the very fine mesh curve at failure.

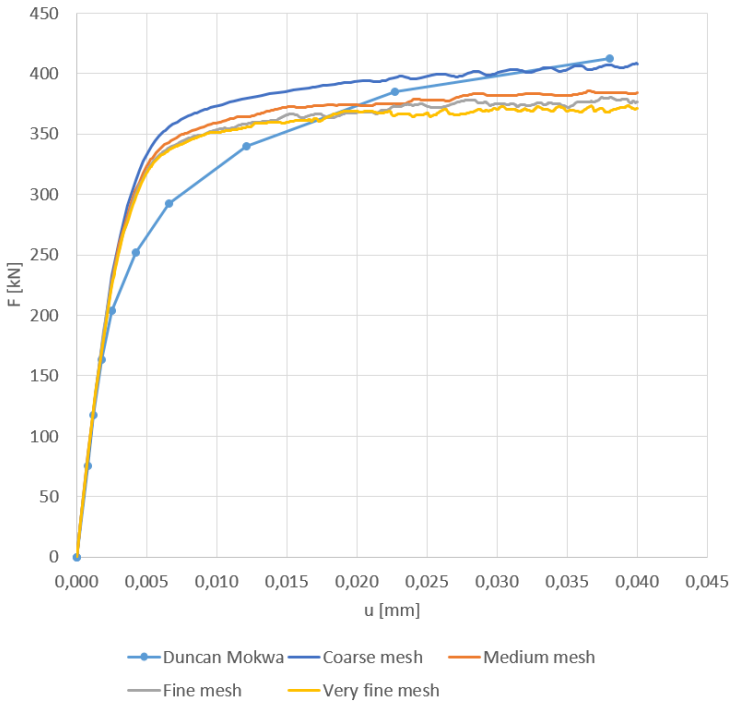

Figure 4.15: Mesh dependency for gravel and natural soil in Plaxis 2D

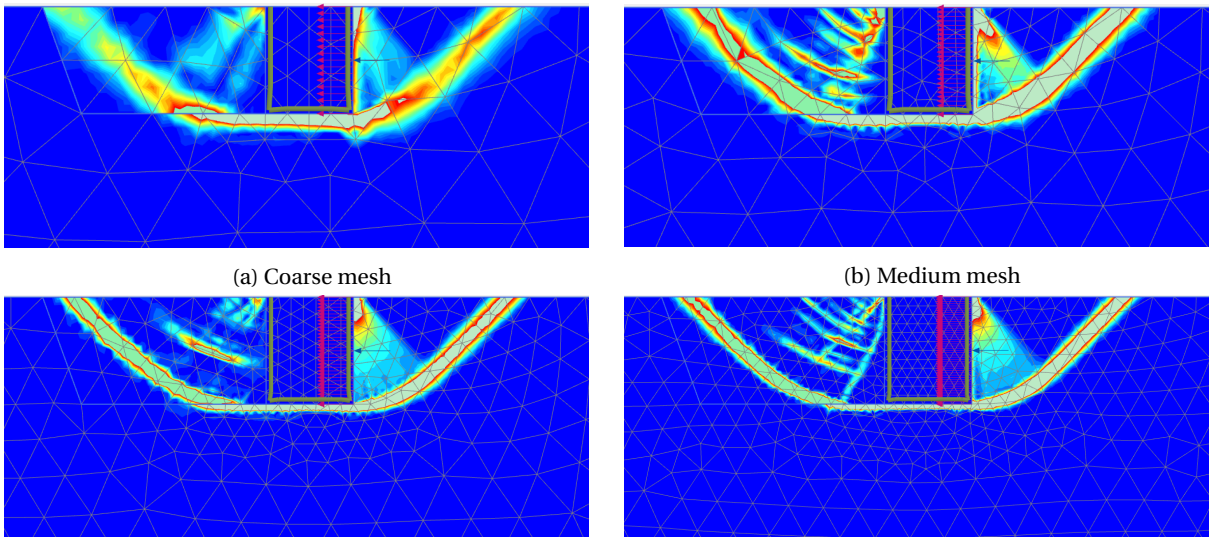

(a) Coarse mesh

(b) Medium mesh

(c) Fine mesh

(d) Very fine mesh

Figure 4.16: Incremental strains for natural soil with gravel backfill

Figure 4.15 gives the load-deflection curves for natural soil with gravel backfill. The curves are identical up to 60% of failure load where they start to deviate. The curve for coarse mesh has an overshoot of 9% compared to the very fine mesh curve. The simulations using medium, fine and very fine mesh are very similar.

Normal- and Shear Stress

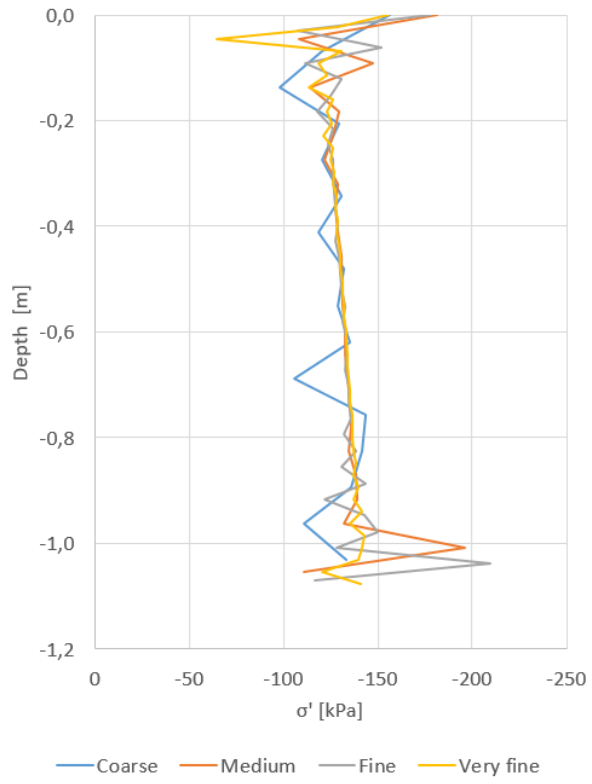

Figure 4.17: Normal stress natural soil

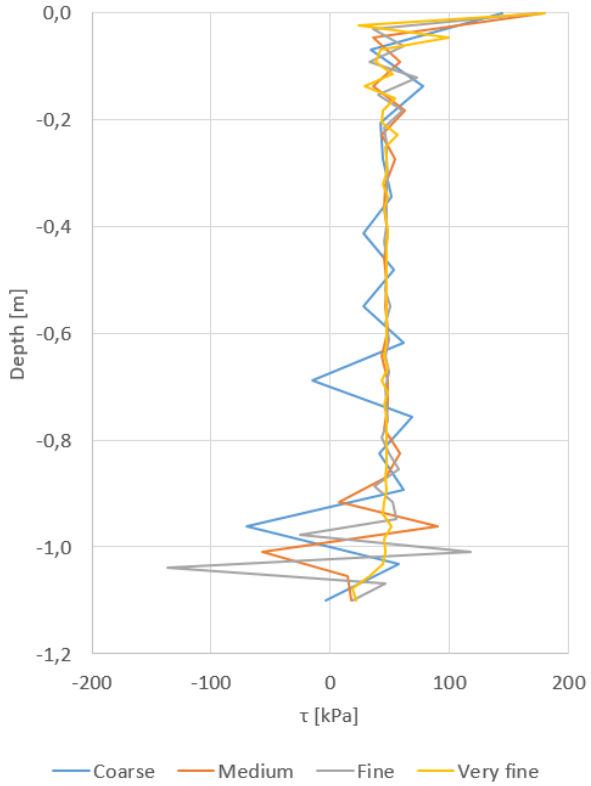

Figure 4.18: Shear stress natural soil

Figure 4.17 displays the normal stress distribution along the concrete wall on passive side for varying mesh sizes for natural soil. From depth 0 to 1 meters the curves show good correlation, with some deviations for the coarse mesh. The normal stress has a slight increase with depth, with a value of about 140 kPa at depth 1 meter.

The shear stress distribution on passive side for varying mesh sizes are displayed in figure 4.18. The curves indicate large shear stresses at the top of the wall, and then a uniform distribution of about 50 kPa. The coarse mesh curve jumps back and forth and shows little correlation with the other obtained curves. The medium and fine curves are erratic at the bottom 20 cm.

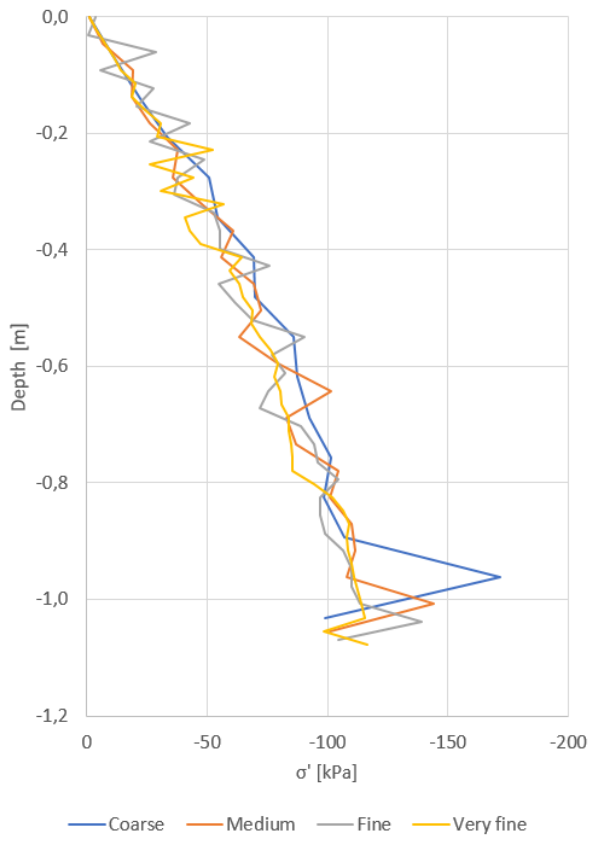

Figure 4.19: Normal stress gravel and natural soil

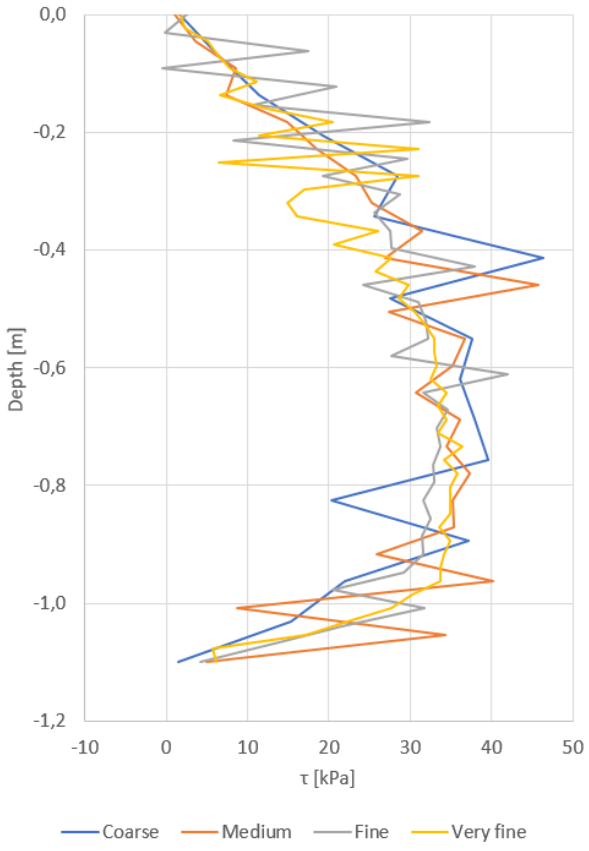

Figure 4.20: Shear stress gravel and natural soil

Figure 4.19 displays the normal stress distribution along the concrete wall on passive side for varying mesh sizes for natural soil with gravel backfill. The curves indicate linear increase with depth from 0 to 0,4 meters, with a slightly smaller increase rate from 0,4 to 1,1 meters. The curves show good correlation. The shear stress distributions in figure 4.20 indicate a nonlinear distribution of shear stress with depth with an average maximum of 35 kPa.

4.5 Plaxis 3D Simulation of Load-Deflection Response

4.5.1 Configuration of Plaxis Model and Boundary Conditions

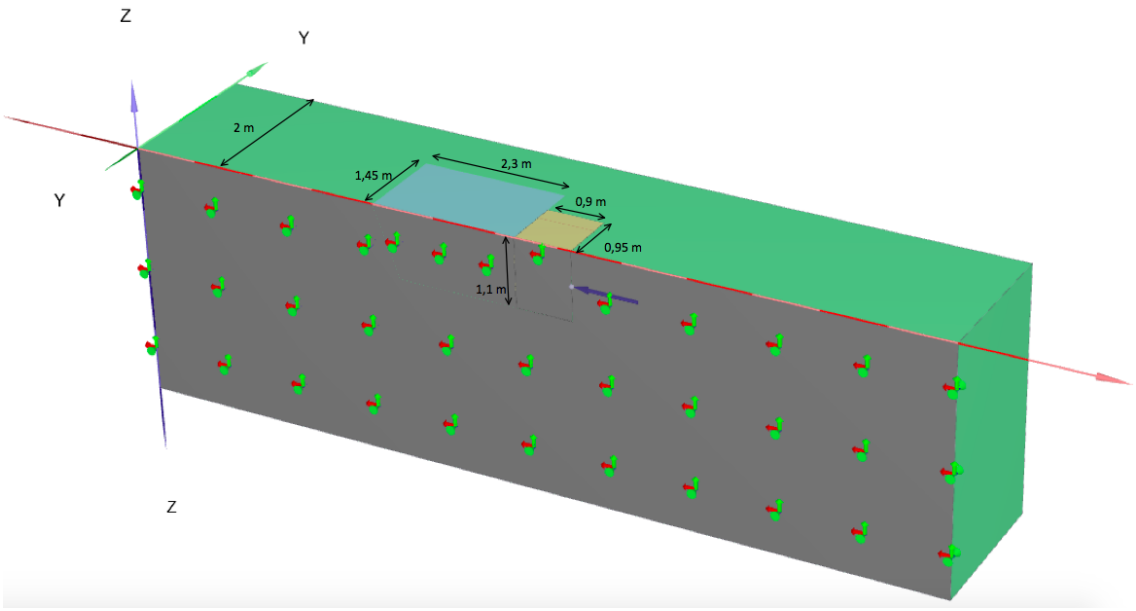

Figure 4.21: Plaxis 3D model

In order to reduce computation time only half of the test setup was modeled (figure 4.21). The model was 13 meters long (x-axis), 4 meters high (z-axis) and 2 meters wide (y-axis). The concrete block and gravel backfill were modeled with width 0,95 and 1,45 meters. The xz-plane was the plane of symmetry. This was modeled by allowing no displacement in y-direction on the xz-plane. The groundwater table was set to depth 4 meters. A prescribed uniform horizontal deformation of 0,04 meters was applied to the concrete block. In the first test the blue soil volume was set to natural soil, and in the second test it was set to gravel. The Mohr-Coulomb Model and the Hardening Soil Model were used. Plaxis 3D Version 2017 was used.

4.5.2 Elements and Mesh

10-node tetrahedral elements were used to model the gravel backfill, natural soil and the concrete wall. The main simulations were run using medium mesh. Additional simulations using coarse and fine mesh were also performed for comparison.

4.5.3 Input Parameters to Finite Element Studies

Table 4.4: Input parameters for modeling of natural soil

Soil	γ $[kN/m^3]$	c [kPa]	ϕ	E' [MPa]	E_{oed} [MPa]	E_{ur}^{ref} [MPa]	m	ψ	ν	R_{int}	R_f	K_0
Natural soil	20	47	0	35	-	-	-	-	0,3	0,75	0,9	automatic
Concrete	23,4	-	-	30 000	-	-	-	-	0,3	0,75	-	-

Table 4.5: Input parameters for modeling of natural soil with gravel backfill

Soil	γ $[kN/m^3]$	c [kPa]	ϕ	E'/E_{50}^{ref} [MPa]	E_{oed} [MPa]	E_{ur}^{ref} [MPa]	m	ψ	ν/ν_{ur}	R_{int}	R_f	K_0
Natural soil	20	35	0	35	-	-	-	-	0,3	0,75	0,9	automatic
Gravel	21,2	0,01	35	100	100	300	0,5	0	0,2	0,75	0,9	1,5
Concrete	23,4	-	-	30 000	-	-	-	-	0,3	0,75	-	-

When modeling the loading against the natural ground, the stiffness E' was reduced by 30% from 50 MPa to 35 MPa to obtain a good fit to the load-deflection curve.

For modeling of the natural soil with gravel backfill, the stiffness parameters for natural soil were found to be too high. In order to obtain a satisfactory solution the parameter c_u was reduced from 50 kPa to 35 MPa, and the stiffness E' was set to 35 MPa. For gravel the friction angle was reduced from 50°to 35°.

4.5.4 Computed Results

Deformed Mesh and Incremental Strains

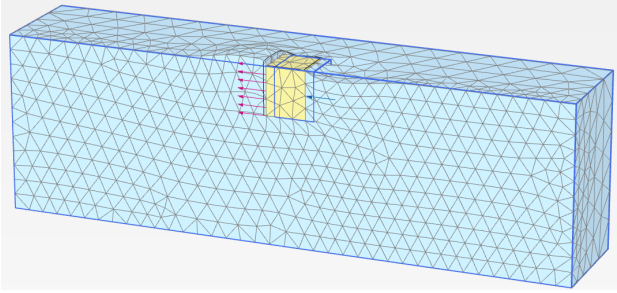

Figure 4.22: Deformed mesh for natural soil

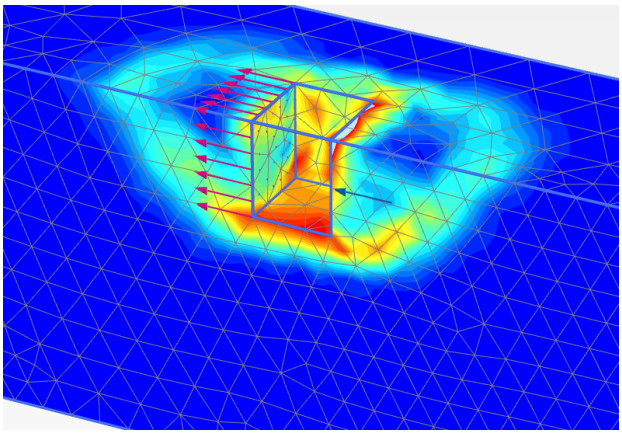

Figure 4.23: Incremental strains for natural soil

Figure 4.22 displays the deformed mesh for wall deformation 4 cm for natural soil. A surface bulge is observed at distance 1,8 meters in front of the wall. In the incremental strain plot in figure 4.23 Rankine zones and rotated skew elements are observed at both sides of the wall.

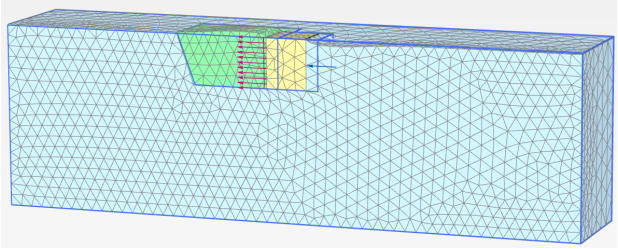

Figure 4.24: Deformed mesh for natural soil with gravel backfill

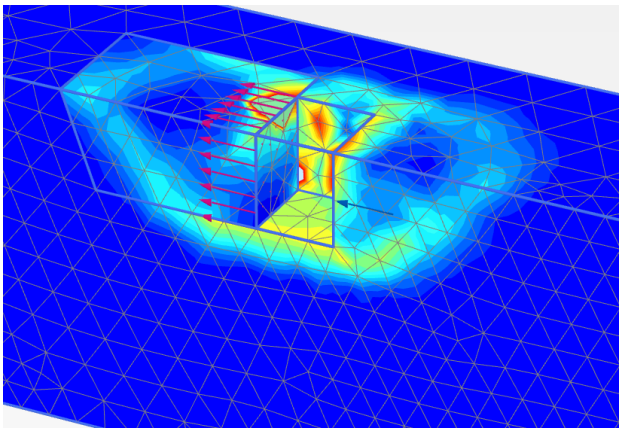

Figure 4.25: Incremental strains for natural soil with gravel backfill

The deformed mesh for natural soil with gravel backfill, figure 4.24 shows a surface bulge at approximately 2,2 meters in front of the block. The incremental strains in figure 4.25 indicate large strains at the right front corner of the block. A passive Rankine zone and rotated skew element are observed in front of the block.

Load-Deflection Curves

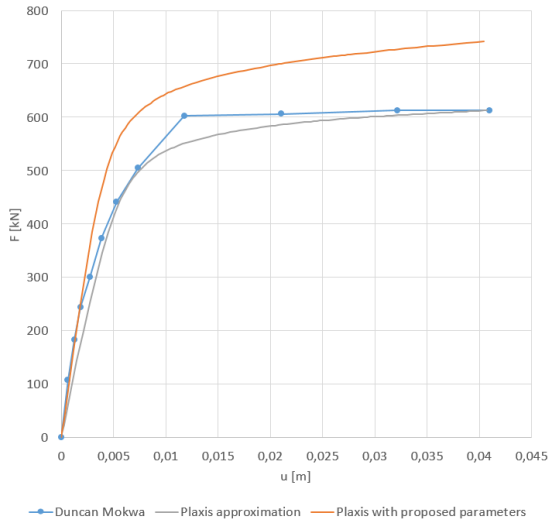

Figure 4.26: Load deflection curve for natural soil

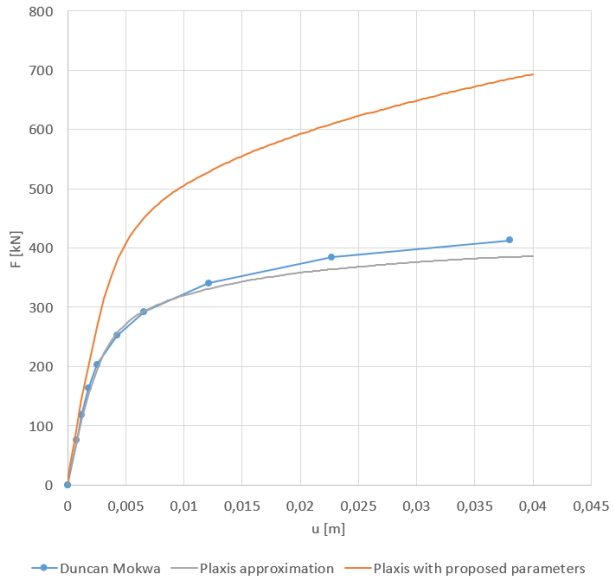

Figure 4.27: Load deflection curve for natural soil with gravel backfill

The computed load-deflection curves for natural soil are shown in figure 4.26. The simulation using previously proposed material parameters gave too stiff behaviour of the soil, with an overshoot at failure of 25%. When using the adjusted input parameters in table 4.4 a very good approximation was made.

Figure 4.27 displays the computed load-deflection curves for natural soil with gravel backfill. For the simulation using parameters obtained from laboratory and calculations, the behavior was too stiff compared to test results, giving a 75% higher failure load. When using the adjusted input parameters in table 4.5 the obtained curve is in good agreement with test results. The simulation gives failure load 5% less than what was observed.

Mesh Dependency

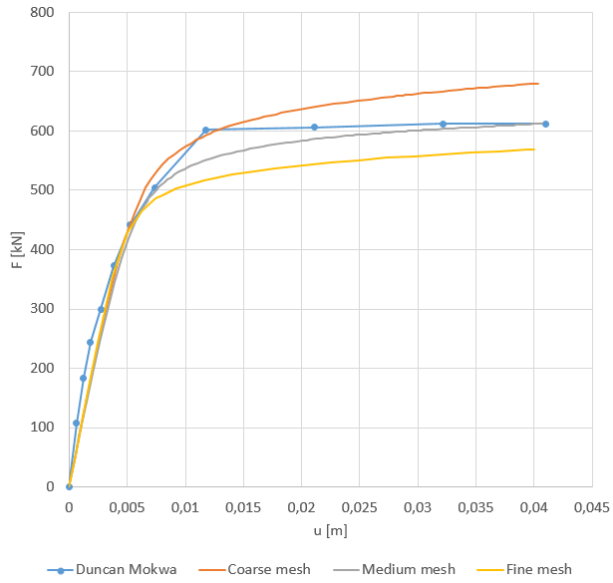

Figure 4.28: Mesh dependency for natural soil

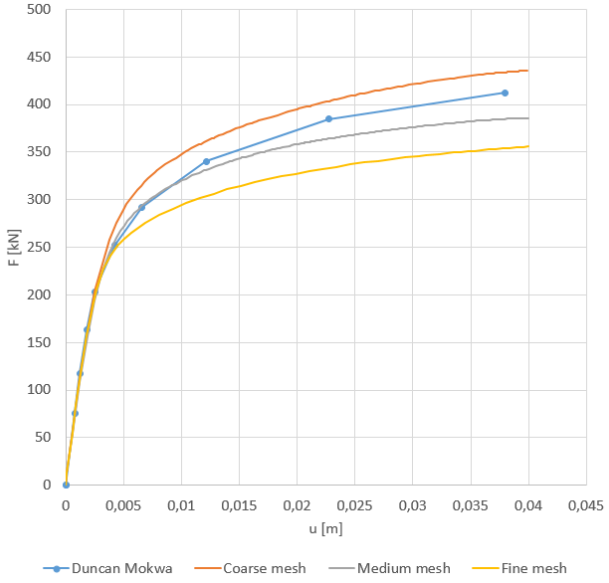

Figure 4.29: Mesh dependency for natural soil with gravel backfill

Figure 4.28 shows the computed load-deflection curves for loading against natural soil, using three different mesh densities. The curves are identical up to 75% of the failure load, then they deviate. The coarse mesh curve has 13% overshoot at failure compared to the field result, and 19 % compared to the fine mesh curve. The incremental strains plots in figure 4.30 are similar for the different mesh sizes. Rankine zones and rotated skew elements are observed on both sides of the block.

The load-deflection curves for varying mesh sizes for natural soil with gravel backfill are displayed in figure 4.29. The curves are identical up to 40% of the failure load, then start to deviate. The fine mesh curve underestimates the failure load by 15%. The coarse mesh curve displays a consistent overshoot of about 8% after deviating. Figure 4.31 shows the incremental strains for natural soil with gravel backfill at failure. The strains look similar for the meshes, with the larges strains at the top and side of the concrete wall. Passive and active Rankine elements can be seen on the left and right side. The failure surface in the gravel appear to be oval in the front.

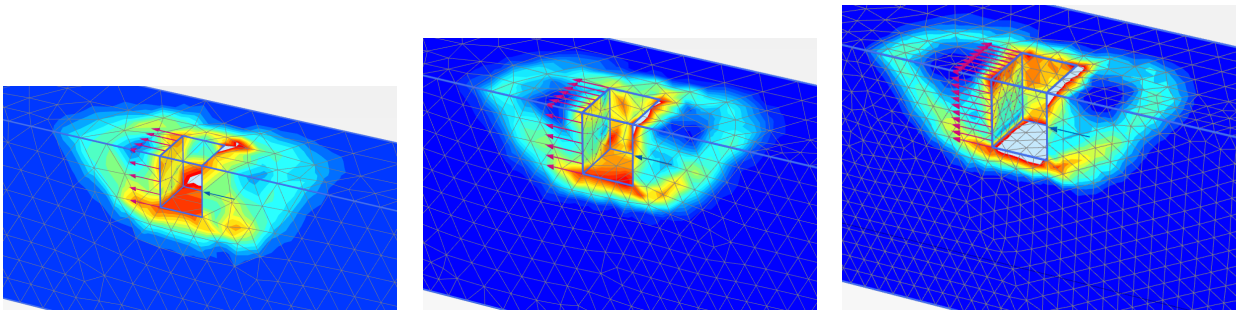

(a) Coarse mesh (b) Medium mesh (c) Fine mesh

Figure 4.30: Incremental strains for natural soil

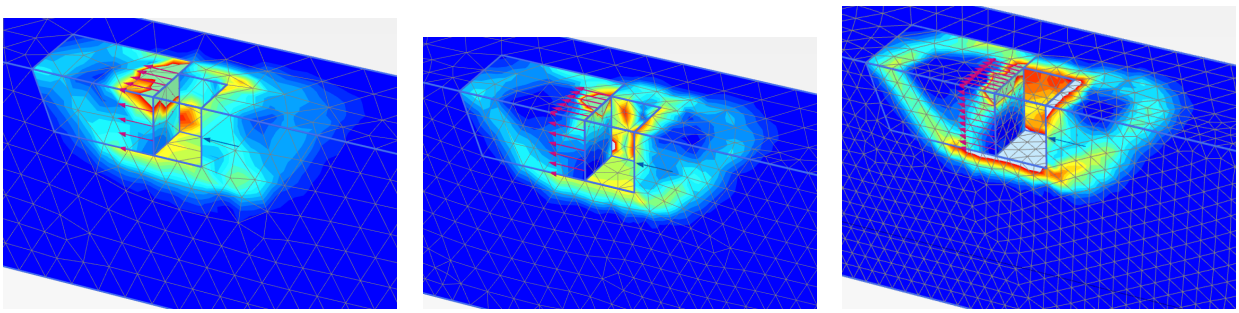

(a) Coarse mesh (b) Medium mesh (c) Fine mesh

Figure 4.31: Incremental strains for natural soil with gravel backfill

Plaxis 2D and 3D Comparison

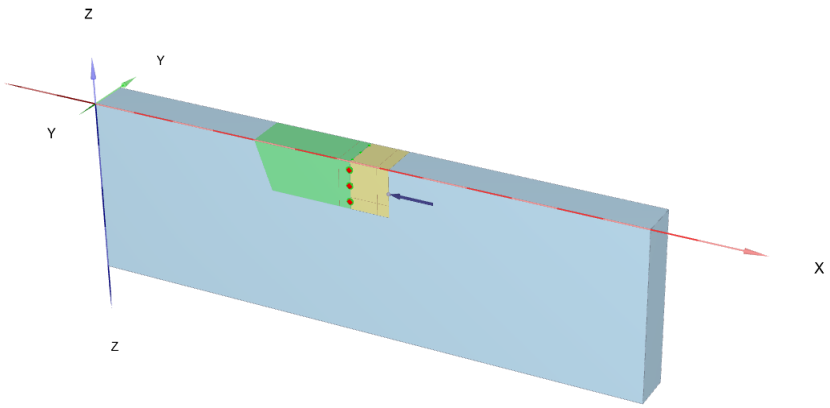

Figure 4.32: 2D modeling in Plaxis 3D

To compare the 2D and 3D calculations a prismatic model with width 0,95 meters was made in Plaxis 3D (figure 4.32). The material parameters from the Plaxis 2D approximation (tables 4.2 and 4.3) were used in both 2D and 3D simulations in this comparison.

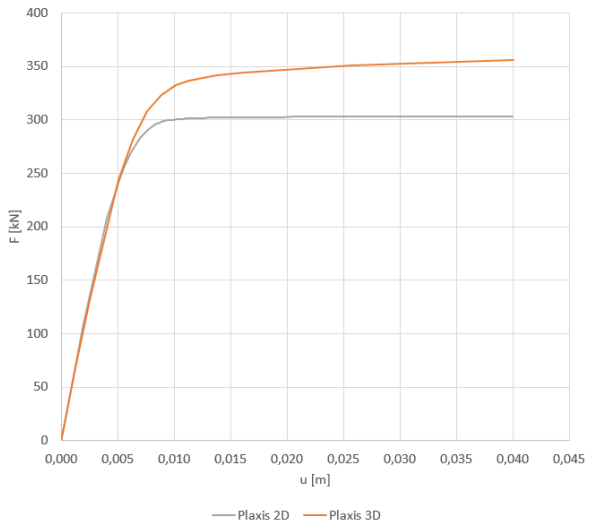

Figure 4.33: Comparison Plaxis 2D and 3D for natural soil

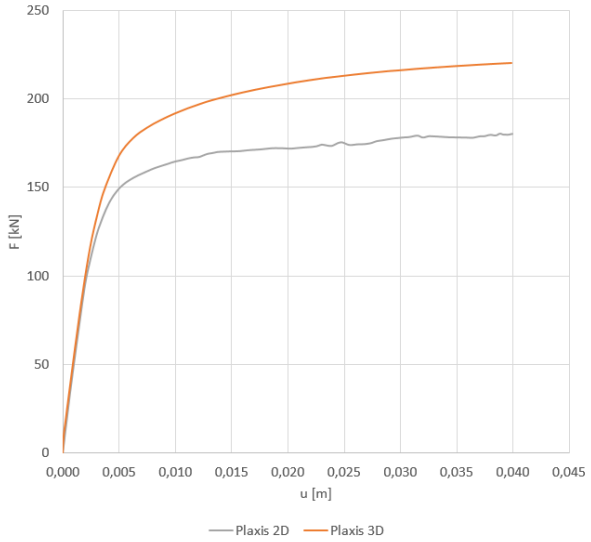

Figure 4.34: Comparison Plaxis 2D and 3D for natural soil with gravel backfill

Figures 4.33 and 4.34 show the comparison between the Plaxis 2D and Plaxis 3D simulations for natural soil and natural soil with gravel backfill, respectively. In both cases the 2D and 3D curves are identical up to 75% of the Plaxis 2D failure load, where they deviate. The Plaxis 3D failure load was 25% larger than that of the Plaxis 2D simulation.

4.6 Hand Calculations

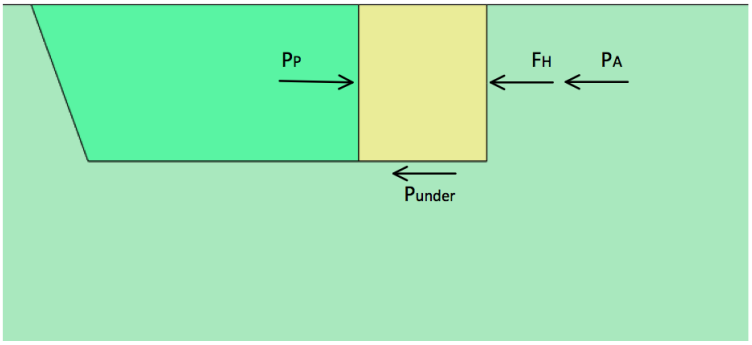

Figure 4.35: Horizontal forces acting on the concrete wall

Figure 4.35 displays the horizontal forces acting on the concrete wall.

Table 4.6: Hand calculation results for natural soil

	r	κ_P	κ_A	P_P [kN]	P_A [kN]	P_{under} [kN]	P_{total} [kN]	δ [mm]
Rankine	0	2	2	219	-173	0	392	5,8
Coulomb	0,75	2	2	219	-173	60	452	12
Janbu	0,75	2,5	2,5	270	-224	60	554	7,1

Table 4.7: Hand calculation results for natural soil with gravel backfill

	r	K_P	κ_A	P_P [kN]	P_A [kN]	P_{under} [kN]	P_{total} [kN]	δ [mm]
Rankine	0	3,7	2	90	-123	0	213	3,9
Coulomb	0,75	13,3	2	320	-123	45	448	10,2
Janbu	0,75	7	2,5	167	-160	45	372	5

The performed hand calculations gave results displayed in tables 4.6 and 4.7. For details of hand calculations see Appendix A.1. Figures 4.36 to 4.39 display the computed passive earth pressures and failure loads. The Janbu theory provided the most accurate results for both cases.

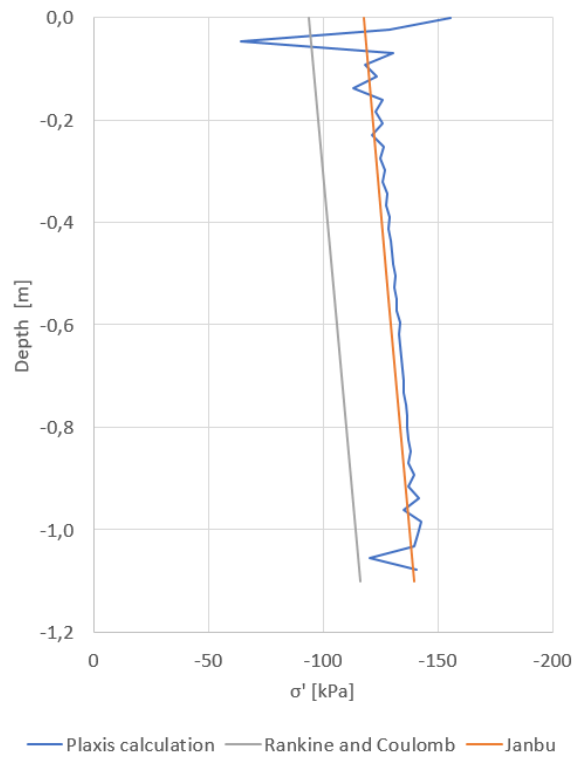

Figure 4.36: Computed passive earth pressure for natural soil

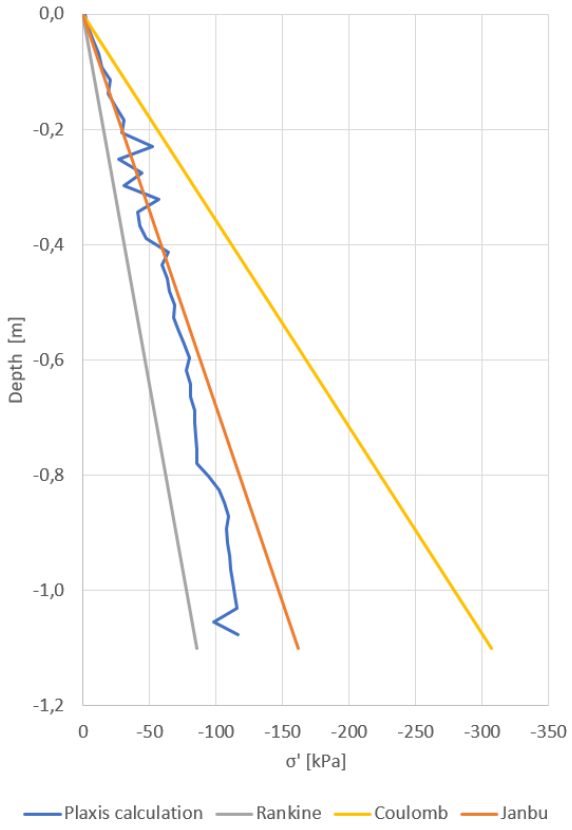

Figure 4.37: Computed passive earth pressure for natural soil with gravel backfill

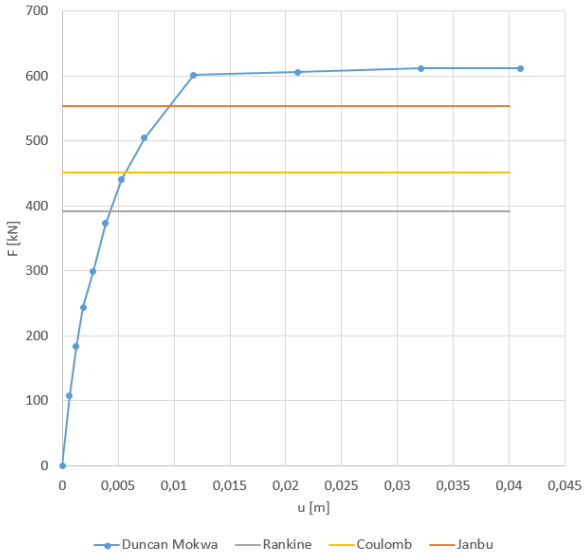

Figure 4.38: Computed failure loads for natural soil

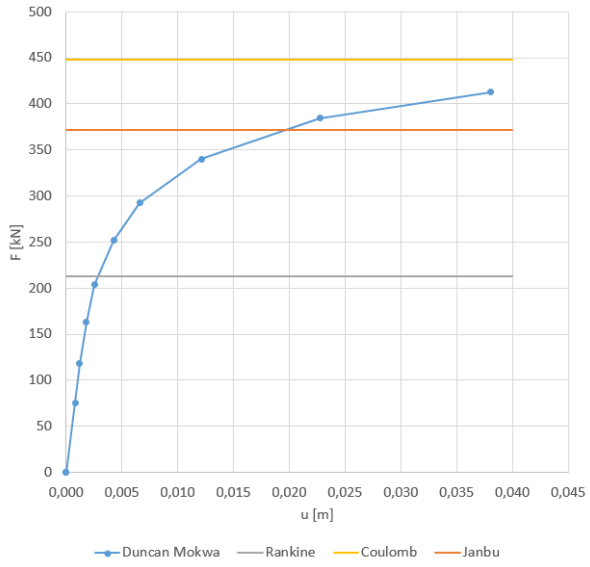

Figure 4.39: Computed failure loads for natural soil with gravel backfill

4.7 Discussion

Load-Deflection Curves and Deformed Mesh

The computed load-deflection curves have been generated using the same material parameters in Plaxis 2D and 3D. For natural soil the parameters from laboratory tests gave relatively good results in Plaxis 2D and an overshoot of 25% at failure for Plaxis 3D. The 3D calculation was expected to give the most accurate results, and it is believed that if the mesh was refined enough it would have. The overshoot in 3D was expected due to the 3D effects as the surrounding soil will support the material behind the wall, and also due to the meshing. For the simulation using a reduced value of E' the 3D simulation gave a curve that better fits with the field results, but the simulation did not go to failure and was stopped at 6 cm deformation. This was however determined to be acceptable as a deformation of more than 6 cm is unlikely for a bridge abutment. The reason for reducing the stiffness parameter E' is the overshoot connected to the meshing. If the mesh was refined enough this adjustment would probably not have been necessary. The deformed meshes show a bulge at distance 1,8 meters in front of the block, which is a good fit to what was observed in the field test.

When simulating the natural soil with gravel backfill using the material parameters as interpreted by the group performing the test gave too high failure load. The main reason for this was the very high friction angle $\phi = 50°$, which was reduced to 35°. To obtain a satisfactory result the undrained shear strenght c_u for the natural soil also had to be lowered. This was unexpected, considering using c_u = 47 kPa gave good results when modeling the natural soil only. A reason for this could be that the natural soil had a loss of shear strength because of remoulding during excavation and the adding of gravel backfill. From the test procedure in the report it appears that after the first test was run the soil in front of the block was excavated and filled with gravel, without being moved to another location. It is therefore believed that the surrounding natural soil has been disturbed after the first test, resulting in a reduction of shear strength. Through trial and error it was discovered that the reference stiffness E_{50}^{ref} for gravel had little influence on the load-deflection curve, as the curve was practically identical for values of E_{50}^{ref} ranging from 30 MPa to 150 MPa (see figure A.3). In other words, the load-deformation correlation for natural soil with gravel backfill seems to be highly dependent on the properties of the surrounding nat-

ural soil. The friction angle of the gravel is however important, as the failure surface mainly goes through the gravel. A friction angle of $\phi = 35°$ was used. In hindsight it is realized that the friction angle for gravel could benefit from a slight increase, as the simulations give failure load 5% less than what was observed in the field. A value of ϕ = 37-38° would probably be more appropriate, which is the empirical value for compacted gravel obtained from Vegdirektoratet (2014).

The relations between wall height and horizontal displacement was found to be δ_h/H = 1% for the case with only natural soil and δ_h/H = 3,4% for the case with natural soil and gravel backfill.

Incremental Strains

The incremental strains are as expected for both the Plaxis 2D and 3D simulations. In the natural soil the Rankine zones are quadratic, as is expected for total stress analysis. The gravel displays a passive Rankine zone, a Prandtl zone and a rotated skew element, as is expected for an a-ϕ analysis. Non-associated flow in the gravel backfill may be the reason for the appearance of several other failure surfaces.

Mesh dependency

For the Plaxis 2D simulations the coarse mesh gives an overshoot of the failure load of about 7% compared to the very fine mesh. The curves for medium, fine and very fine mesh are very similar. The difference in meshing appear to have greater significance for the Plaxis 3D simulations. As shown in figures 4.28 and 4.29 the medium and coarse mesh has around 10% and 20% overshoot compared to the fine mesh curve. The relatively large difference in failure load for different meshing in Plaxis 3D was expected, due to the three dimensional elements. The 10-node tetrahedral used in Plaxis 3D (figure 3.3) is an element of second order, and will not provide the same accuracy as the fourth order 15-node triangles used in Plaxis 2D (figure 3.2).

Normal- and Shear Stresses

For natural soil the normal stresses in figure 4.17 display a linear increase with depth, with 115 kPa at the top and 140 kPa at the bottom. This is a good fit to the hand calculations. The shear stresses in figure 4.18 indicate a uniformly distributed shear stress of 47 kPa along the wall. This is equal to the undrained shear strength s_u, and this value would be expected if the input param-

eter R_{int} was set to 1. As table 4.2 shows, R_{int} was set to 0,75 for all materials in this simulation and hence the shear stress was expected to be 35 kPa. This is an indication of issues with the interfaces along the wall, but the cause of the problem was not determined.

The normal stresses along the wall for gravel (figure 4.19) display a practically linear distribution with depth. From 0,4 to 1,1 meters the increase is slightly smaller. This could be caused by a minor rotation about the base of the concrete block, but this type of distribution can also occur for purely horizontal wall movement, as shown by Fang et al. (1994). The shear stress distribution in figure 4.20 is definently nonlinear, which also could be a consequence of the wall movement.

Plaxis 2D and 3D Comparison

When using a prismatic model in Plaxis 3D figure 4.32 indicate a 25% overshoot compared to Plaxis 2D. The 25% Plaxis 3D overshoot is partly explained by the difference in the meshing. Both simulations were run using medium mesh, but the meshes were not identical. The Plaxis 3D mesh was coarser along the wall, with only three elements over the wall height compared to the six elements for Plaxis 2D. Also the poor quality of the three dimensional Plaxis 3D elements is expected to have increased the overshoot.

Hand Calculations

The hand calculations were performed using the theories of Rankine, Coulomb and Janbu. The presence of active earth pressure was confirmed by viewing the tension cut-off points in Plaxis (figure A.2). The Rankine theory is only applicable for wall roughness $r = 0$, which is the reason for the small computed earth pressure and failure load. As argued by Duncan and Mokwa (2001), the Coulomb model gives passive earth pressures too high for values of $\delta > 0,4\phi$. The model is considered conservative as it assumes a plane failure surface. In this case $\delta = 28^\circ = 0,8\phi$, and the computed passive earth pressure is confirmed to be too high. The theory of Janbu assumes a curved failure surface near the wall, making it less conservative. The computed passive earth pressure using Janbu's theory fits well with that of the Plaxis simulations, but because it assumes a linear distribution there is some deviation at the bottom.

Chapter 5

Case 2: Wilson and Elgamal (2010)

5.1 Test Procedure

Two passive earth pressure tests (Wilson and Elgamal, 2010) were conducted in a large soil container at the University of California, San Diego. One test was conducted with the backfill close to its placement water content, while the other test was performed in a drier condition. In this case study only the test performed in a drier condition will be back-calculated. The test arrangement is shown in figure 5.1. A large laminar box was restrained from translation by two steel towers. The inside walls were covered by smooth low friction plastic sheets in order to minimize the friction between the soil and the sides of the container. The sand backfill was placed in small lifts and compacted.

The test wall was made of reinforced concrete, and was essentially rigid. The wall was 2,13 meters high, 2,74 meters wide and 0,2 meters thick. To keep the wall stable during construction and testing, the wall was suspended from a beam which rested on rollers. The combined mass of the test wall and the supporting beam was 4500 kg, equal to weight of 15,4 kN/m^3.

The load was applied to the test wall using four hydraulic jacks. To maintain a uniform field of lateral wall displacement, the jacks were connected to a hydraulic pump, allowing for independent control.

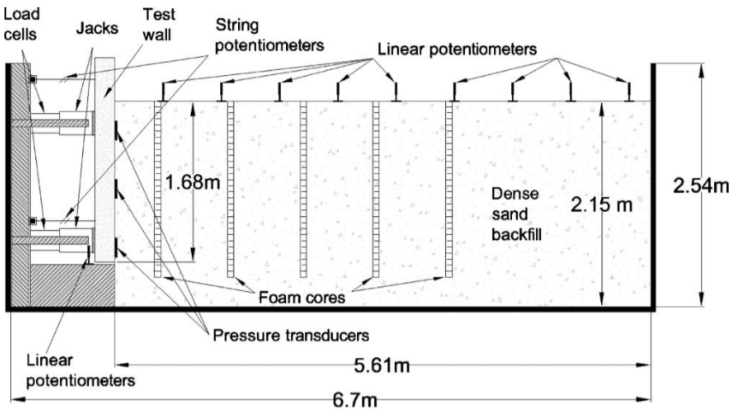

Figure 5.1: Test arrangement for passive pressure load tests (foam cores were not used in this test) (Wilson and Elgamal, 2010)

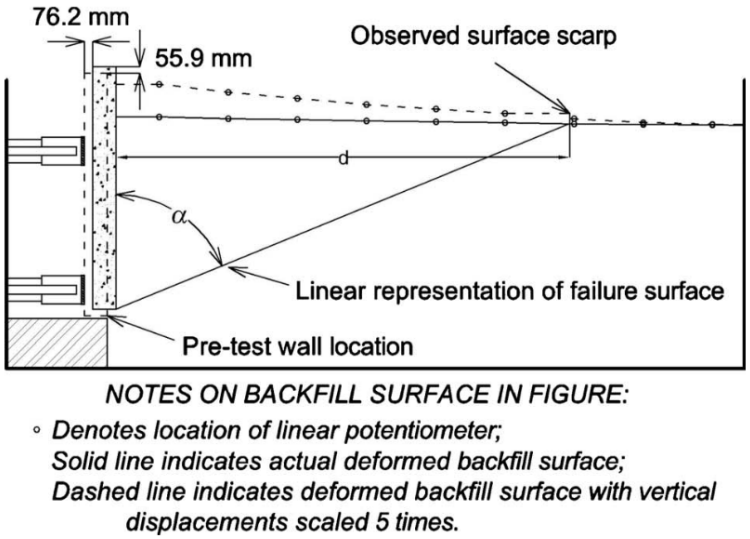

Figure 5.2: Profile of passive failure wedge from load test (Wilson and Elgamal, 2010)

5.2 Soil Properties

The backfill material was tested in the laboratory to obtain material parameters. Soil classification tests indicated that the soil consisted of sand with nonplastic silt (about 7%) and gravel (about 7%). Direct shear and triaxial compression tests were performed, and the results are displayed in table 5.1.

Table 5.1: Material properties

Soil	γ $[kN/m^3]$	c [kPa]	ϕ'	c_r [kPa]	ϕ'_r
Sand	20,6	14	48	6	35

The secant modulus to 50% of the peak stress (E_{50}) was estimated to be 16,4 MPa, 18,7 MPa and 48,2 MPa for 37, 72 and 144 kPa cell pressures, respectively.

5.3 Computation of Stiffness Parameters

The relations obtained in section 4.3 are used to calculate the stiffness parameters in this section.

The proposed soil properties from the group performing the test indicate a cohesion $c = 14kPa$, corresponding to an attraction $a = 13,5kPa$. k_{50} is found from the load-displacement curve in figure 5.3, see equation 5.1. The backfill is compacted, which may cause an increase of the earth pressure coefficient K'_0, which is assumed to be 1,5. The index m is set to 0,5 for the backfill.

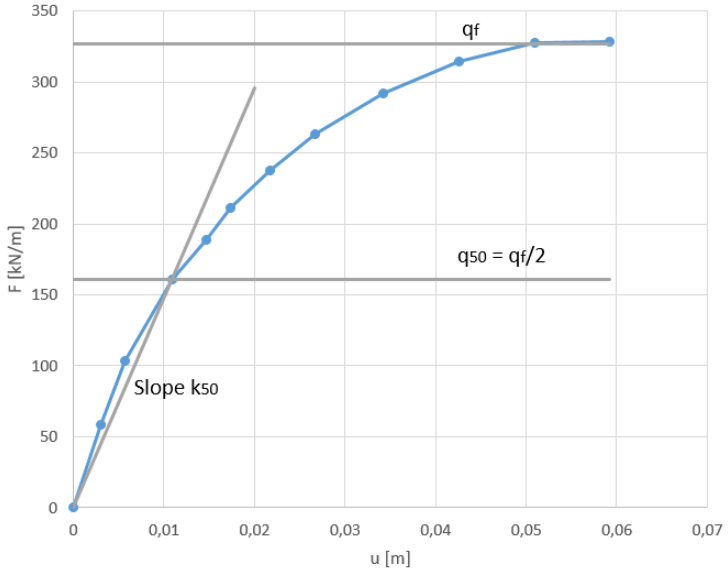

Figure 5.3: Test arrangement for passive pressure load tests (foam cores were only used in Test 1) (Wilson and Elgamal, 2010)

$$k_{50} = \frac{q_{50}}{u_{50}} = \frac{161kN}{10,9mm} = 14,8kN/mm \tag{5.1}$$

$$\bar{E} = \frac{2k_{50}}{W} = \frac{2 * 14,8kN/mm}{2740mm} = 10,8MPa \tag{5.2}$$

$$E_{50}^{ref} = \bar{E}_{50}\left(\frac{p'_{ref} + a}{\sigma'_3 + a}\right)^{1-m} = 10,8MPa\left(\frac{100kPa + 13,5kPa}{1,5 \cdot 17,3kPa + 13,5kPa}\right)^{0,5} = 18,3MPa \tag{5.3}$$

5.4 Plaxis 2D Simulation of Load-Deflection Response

5.4.1 Configuration of Plaxis model and boundary conditions

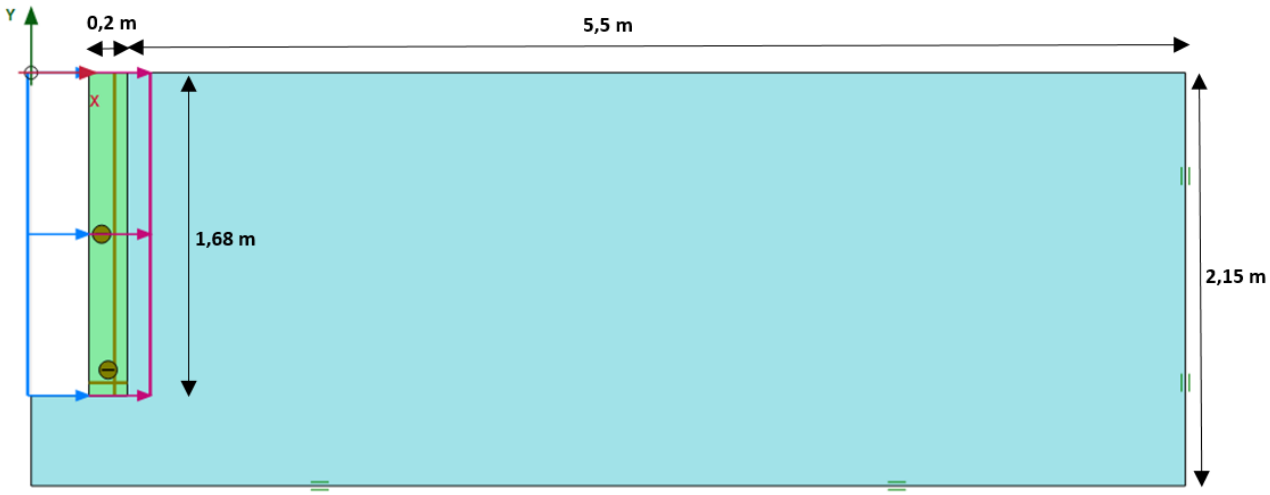

Figure 5.4: Plaxis 2D model

A plane strain FE model was calibrated based on the load test and lab data from the experiment. The boundary conditions and dimensions of the model were set to match the test configuration (5.4). The model was 6 meters wide ($x_{min} = 0$, $x_{max} = 6m$) and 2,15 meters high ($y_{min} = -2,15$, $y_{max} = 0$). The concrete wall had dimensions $0,2mx1,68m$. The groundwater table was set to depth 2,15 meters. Interfaces were created along the concrete wall to account for the soil-structure interaction. A prescribed horizontal displacement $u = 0,06m$ was applied to the wall in order to maintain a uniform field of lateral wall displacement. In order to simulate the laminar box, the soil was restricted from vertical displacement in the bottom, and from horizontal displacement at the end. The Hardening Soil Model was used. Plaxis 2D Version 2016.01 was used.

5.4.2 Elements and Mesh

Triangular 15-node elements were used to model the gravel, natural soil and the concrete block. The main simulations were run using a fine mesh. Additional simulations with coarse, medium and very fine meshes were also performed for comparison.

5.4.3 Input Parameters to Finite Element Studies

Table 5.2: Input material parameters

Soil	γ $[kN/m^3]$	c [kPa]	ϕ'	E_{50}^{ref} [MPa]	E_{oed} [MPa]	E_{ur}^{ref} [MPa]	m	ψ	υ_{ur}	R_{int}	R_f	K_0
Backfill	20,6	5	30	18	18	60	0,5	0	0,2	0,75	0,9	1,5
Concrete	15,4	-	-	30 000	-	-	-	-	0,3	0,75	-	-

In order to obtain a satisfactory load-displacement curve the angle of friction was reduced from 48° to 35°. Also, the cohesion was reduced from 14 kPa to 5 kPa.

5.4.4 Computed Results

Deformed Mesh and Incremental Strains

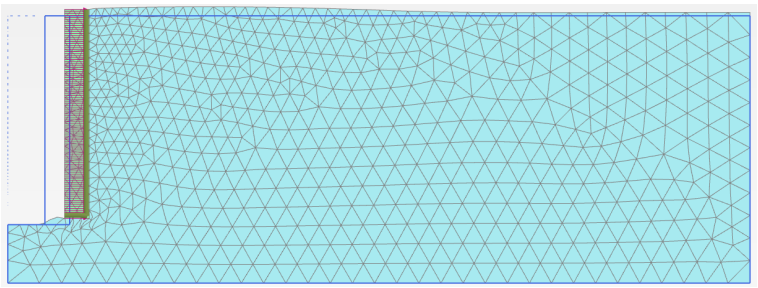

Figure 5.5: Deformed mesh

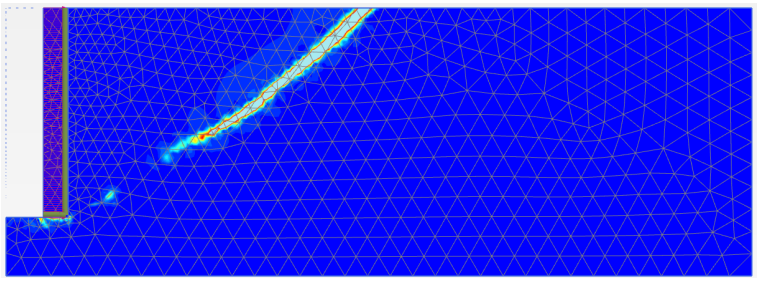

Figure 5.6: Incremental strains

Figure 5.5 displays the deformed mesh at failure, for wall deformation 4 cm. The wall has been lifted 5 cm upwards, and a bulge is observed at the surface 3 meters in front of the wall. The incremental strains at failure are given in figure 5.6. A Passive Rankine failure element is observed.

Load-Deflection Curve

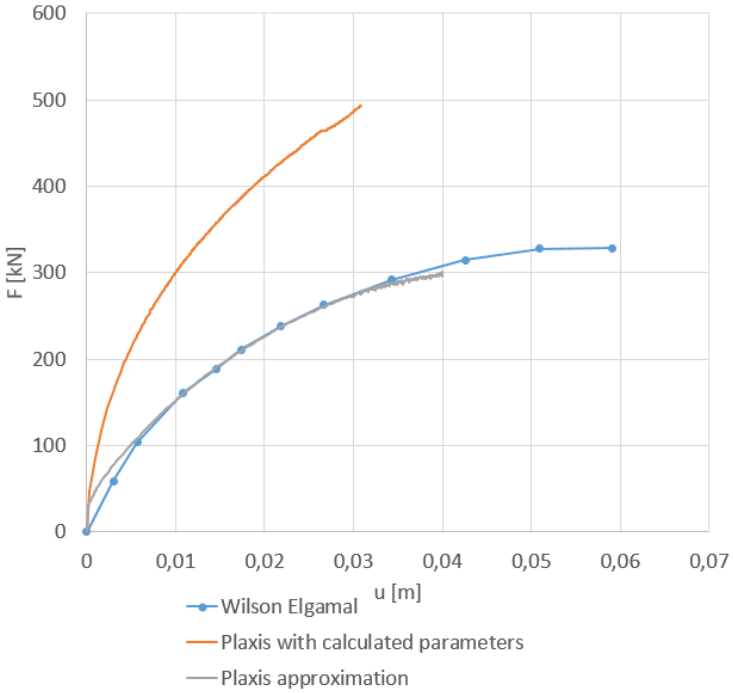

Figure 5.7: Load-deflection curve

Figure 5.7 displays the obtained load-deflection curves. Using the material parameters obtained from laboratory tests and the calculated E_{50}^{ref} (Plaxis with calculated parameters curve) the soil behaviour was to stiff. The obtained Plaxis approximation is a good fit up to 90% of the field test failure load, where it stops.

Mesh Dependency and Incremental Strains

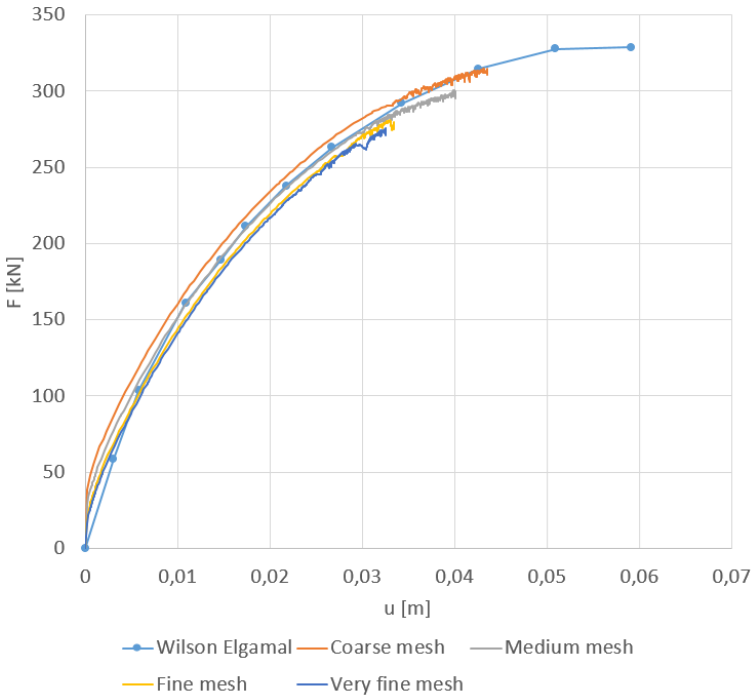

Figure 5.8: Mesh dependency

Figure 5.8 displays load-deflection curves for different mesh sizes using the parameters in table 5.2. The curves indicate increasing overshoot with increasing mesh coarseness, with about 7% overshoot for the coarse mesh compared to the very fine mesh.

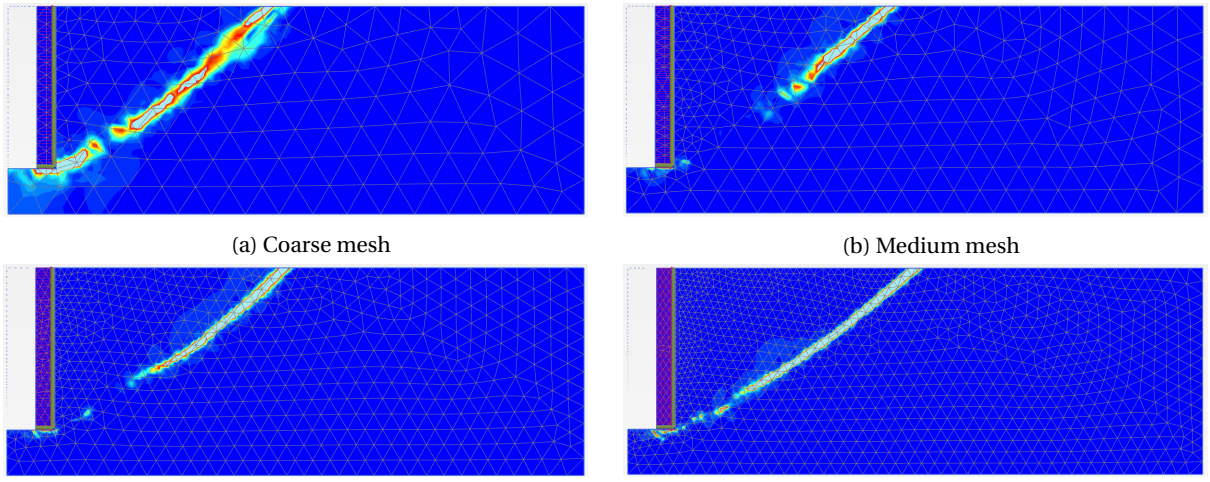

(a) Coarse mesh

(b) Medium mesh

(c) Fine mesh

(d) Very fine mesh

Figure 5.9: Incremental strains

Figure 5.9 show the incremental strains for different mesh densities at failure. The failure

surface looks to be relatively straight for all the mesh densities, with a slight curvature.

Normal- and Shear Forces

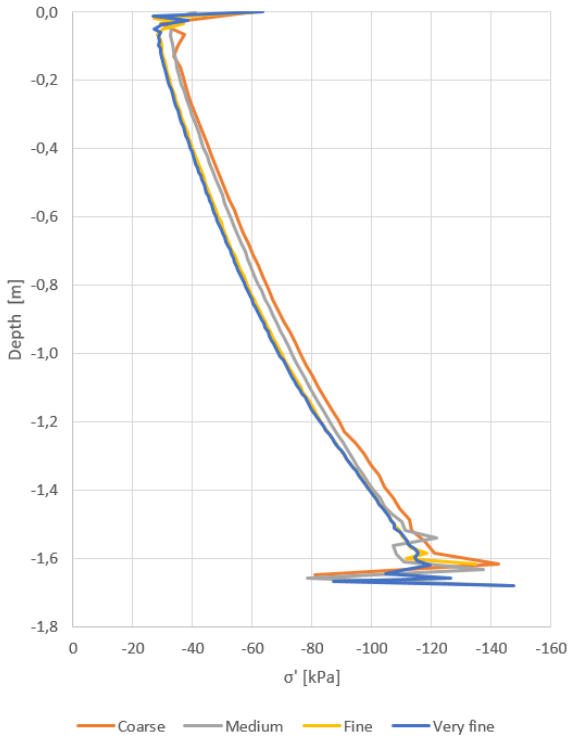

Figure 5.10: Normal stress acting on wall at failure

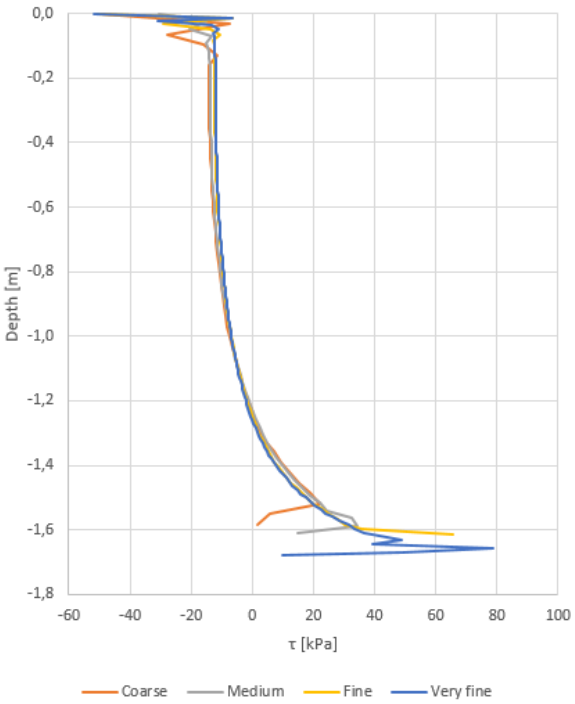

Figure 5.11: Shear stress acting on wall at failure

The normal stresses acting on the wall at failure are displayed in figure 5.10. The normal stress increases almost linearly with depth. The curves indicate normal stress 30 kPa at the top and about 120 kPa at the bottom of the wall. The coarse mesh gives the highest stresses with about 10 kPa difference from the very fine mesh.

Figure 5.11 shows the shear stresses acting on the wall at failure. The curves indicate negative shear stresses from depth 0 to 1,2 meters, and positive stresses from 1,2 to 1,7 meters. Near the top the shear stress is -10 kPa and at the bottom it is between 60 and 80 kPa.

5.5 Plaxis 3D Simulation of Load-Deflection Response

5.5.1 Configuration of Plaxis Model and Boundary Conditions

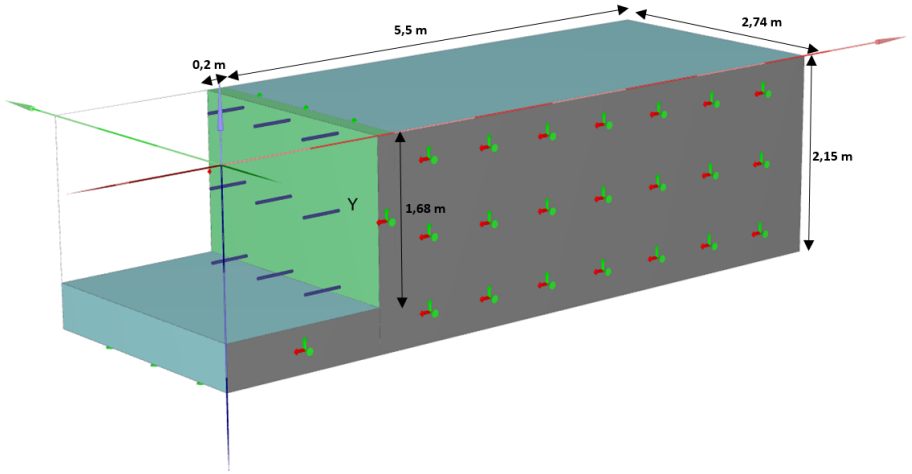

Figure 5.12: Plaxis 3D model

Figure 5.12 displays the Plaxis 3D model. The modelled backfill was 5,5 meters long (x-axis), 2,15 meters high (z-axis) and 2,74 meters wide (y-axis). The concrete wall was 0,2 meters long and 1,68 meters high. The groundwater table was set to the bottom of the model. Interfaces were created along the concrete wall to account for soil-structure interaction. A uniformly distributed load acted along the wall. A prescribed uniform horizontal displacement of 0,06 meters was applied to the wall. In order to simulate the laminar box, the soil was restricted from displacement out of the plane along the sides, the back and the bottom. The Hardening Soil Model was used. Plaxis 3D Version 2017 was used.

5.5.2 Elements and Mesh

10-node tetrahedral elements were used to model the backfill and concrete wall. The main simulations were run using medium mesh. Additional simulations using coarse and fine mesh were also performed for comparison.

5.5.3 Input Parameters to Finite Element Studies

Table 5.3: Input parameters for modeling of gravel

Soil	γ $[kN/m^3]$	c [kPa]	ϕ'	E_{50}^{ref} [MPa]	E_{oed} [MPa]	E_{ur}^{ref} [MPa]	m	ψ	υ_{ur}	R_{int}	R_f	K_0
Gravel	20,6	5	30	18	18	60	0,5	0	0,2	0,75	0,9	1,5
Concrete	15,4	-	-	30 000	-	-	-	-	0,3	0,75	-	-

In order to obtain a satisfactory solution the parameters in table 5.3 were used. The angle of friction ϕ' was reduced from 48° to 30°, and the cohesion c was reduced from 14 kPa to 5 kPa. The computed E_{50}^{ref} was found to be appropriate.

5.5.4 Computed Results

Deformed Mesh and Incremental Strains

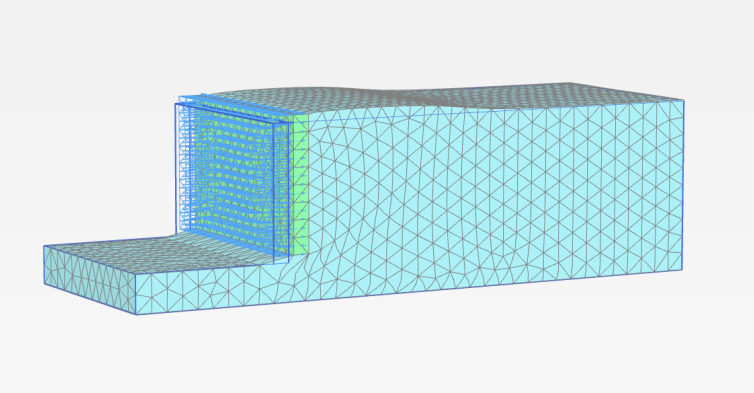

Figure 5.13: Deformed mesh

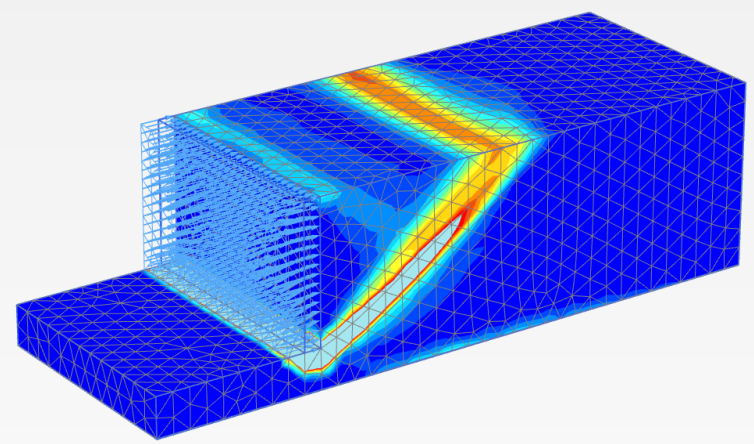

Figure 5.14: Incremental strains

Figure 5.13 shows the deformed mesh at failure, for a wall deformation of 6 cm. The wall has an upwards vertical displacement of 8 cm. A bulge is observed at the surface 2,7 meters in front of the wall. The incremental strains for the medium mesh simulation are plotted in figure 5.14. A relatively planar failure surface is observed, with a rotated skew element.

Load-Deflection Curve

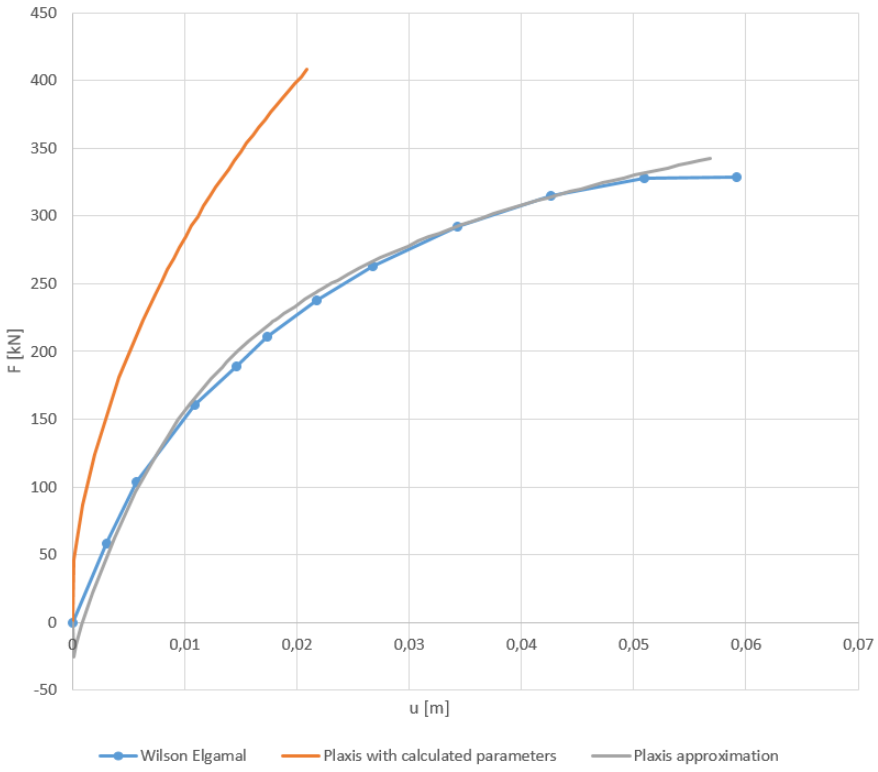

Figure 5.15: Load-deflection curve

The load-deflection curve in figure 5.15 show that the material parameters obtained from laboratory tests gave too stiff soil behavior. Using the parameters in table 5.3 a good fit for the load-deflection curve was made. The Plaxis load test was stopped at 6 cm deformation and did not go to failure. Note that the deformation curve dips down to -20 kN at the beginning of the loading test.

Mesh Dependency

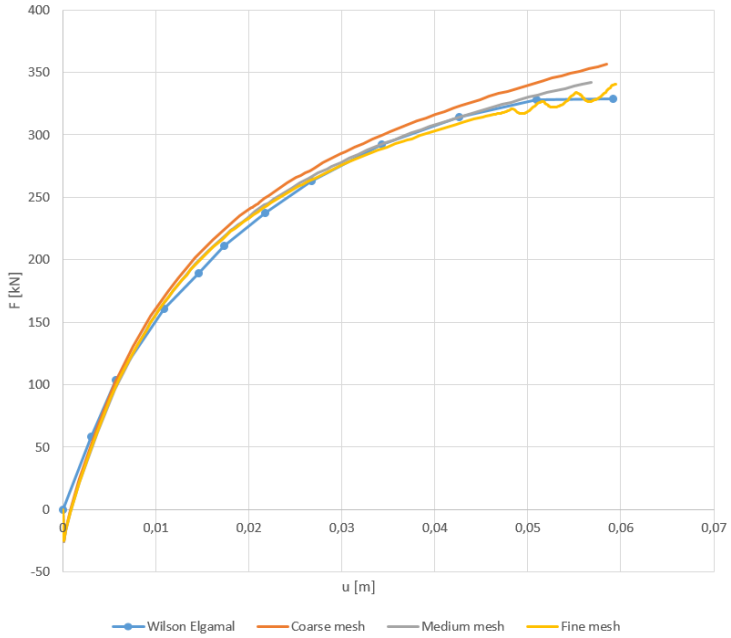

Figure 5.16: Mesh dependency

The load-deflection curves given in figure 5.16 are identical up to 40% of failure load, where they start to deviate slightly. The coarse mesh displays 7% overshoot at failure compared to the fine mesh curve.

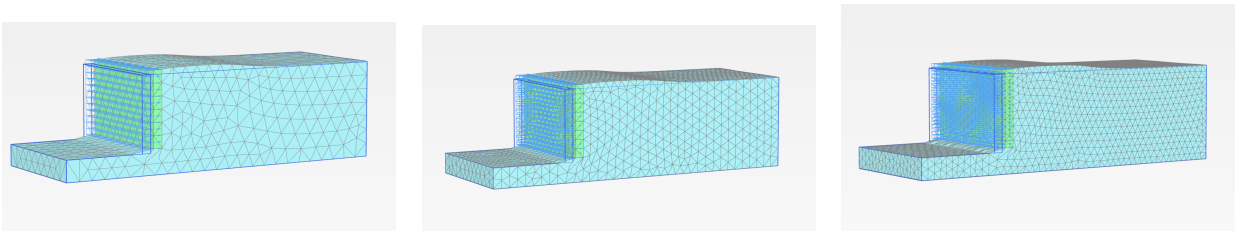

(a) Coarse mesh (b) Medium mesh (c) Fine mesh

Figure 5.17: Deformed mesh

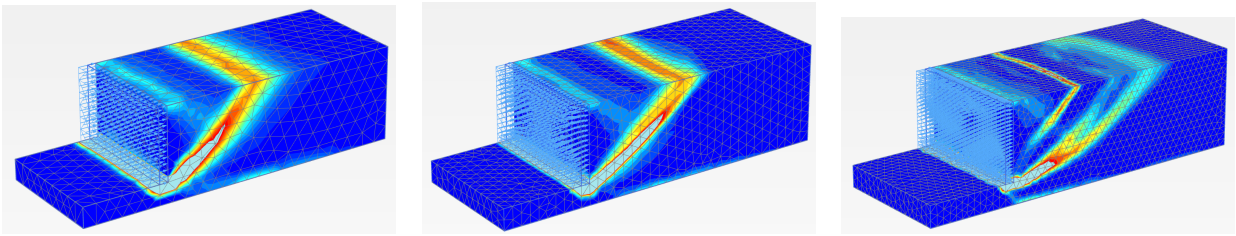

(a) Coarse mesh (b) Medium mesh (c) Fine mesh

Figure 5.18: Incremental strains

Figure 5.17 shows the deformed meshes and figure 5.18 shows the incremental strains. For the coarse and medium mesh a planar failure surface and a rotated skew element is observed. In the fine mesh the failure surface is more curved and several other failure surfaces are observed.

Plaxis 2D and 3D Comparison

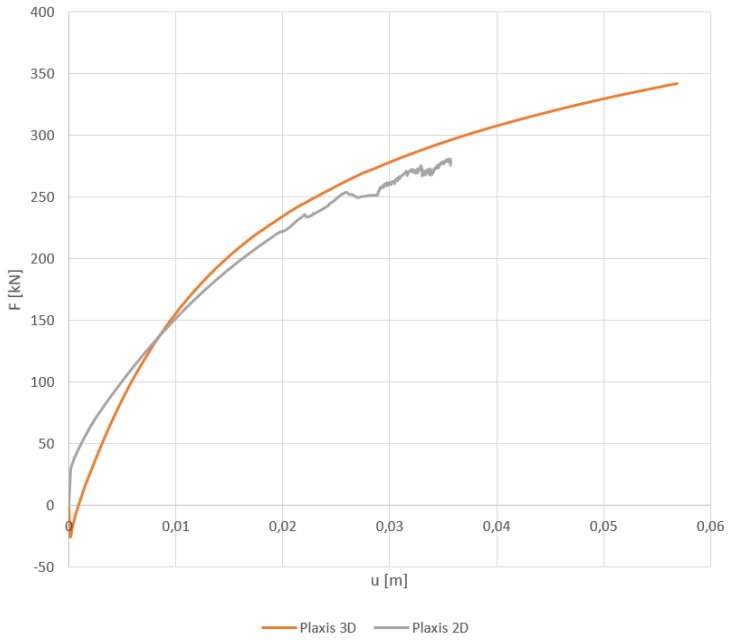

Figure 5.19: Fine mesh

Figure 5.19 shows the load deflection curves for Plaxis 2D and Plaxis 3D, using the material parameters from table 5.2 and medium mesh. The two curves are in good agreement up to 35 mm deformation, where the Plaxis 2D simulation stops.

5.6 Hand Calculations

Figure 5.20: Horizontal forces acting on the wall

Table 5.4: Results of hand calculations

	r	K_P	P_P [kN]	P_{total} [kN]	δ [mm]
Rankine	0	3	331	331	8,1
Coulomb	0,75	7	704	704	17,1
Janbu	0,75	4,5	455	455	11,1

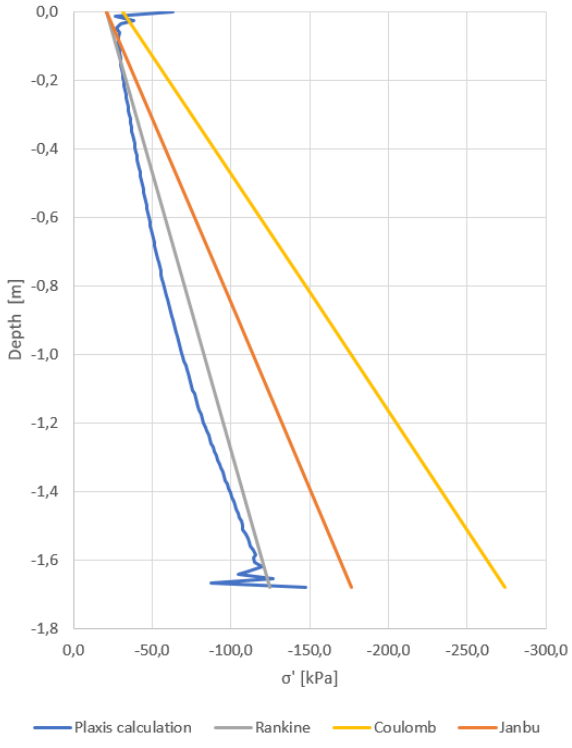

Figure 5.21: Computed passive earth pressure

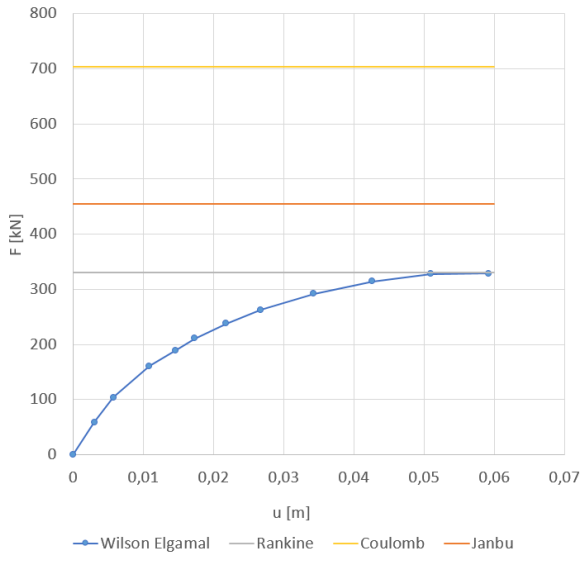

Figure 5.22: Computed failure loads

Table 5.4 shows the results of performed hand calculations using earth pressure theories of Rankine, Coulomb and Janbu, and figure 5.22 shows the computed failure loads. The procedure of the hand calculations can be viewed in Appendix B.1. Figure 5.21 show the calculated passive earth pressures acting on the wall. The Rankine Theory provides a good fit to what was calculated using Plaxis 2D.

5.7 Discussion

Load-Deflection Curves and Deformed Mesh

For both the Plaxis 2D and 3D simulations the parameters obtained from laboratory tests gave too stiff behaviour. This was mainly because of the high friction angle ϕ=50°, which was quite unrealistic. Lowering the angle of friction to 30° gave good results. A friction angle of 30° is in the lower range of empirical values for sand, but when viewed in context with the relatively low stiffness it was found to be appropriate. A cohesion of c = 5 kPa was found to be appropriate. The test report states that the sand was compacted, but imperical values indicate that a well compacted sand should display a higher stiffness, friction angle and cohesion. The soil is therefore assumed to be poorly compacted, which could explain the low values. Due to the lack of raw data from the experiment this was not investigated further.

The Plaxis 2D simulations stopped at 80-90% of the failure load observed in the field due to numerical issues. This was however determined to be acceptable because the behaviour in the small strains range are the most important for dimensioning of bridge abutments.The load-deflection curve from the Plaxis 3D simulation (figure 5.15) is in good agreement with the field load test. The simulation did not go to failure, but was stopped at deformation 6 cm. The obtained curve does indicate a negative load step to -20 kN at the beginning. The reason for this is not known, and there is a possibility that this could have affected the accuracy of the results. The deformed meshes for Plaxis 3D indicate a 8-9 cm uplift of the wall at failure, which is more than the field test which gave 55,9 mm vertical uplift. This is could indicate that the model is not working correctly.

The relation between wall height and horizontal displacement at failure was found to be δ_h/H

= 3% for the sand backfill.

Incremental Strains

For Plaxis 2D the incremental strains indicate a plane shear surface, and a Passive Rankine failure zone is observed. A rotated skew element was expected to appear, but it did not. A reason for this could be that the simulations stopped at deformation 3-4 cm, and the strains were too small for the skew element to develop. In the 3D simulations deformation of 6 mm was obtained, and for the coarse and medium mesh a plane shear surface is observed, in addition to a Passive Rankine zone and a rotated skew element. For the fine mesh several failure surfaces appear, indicating non-associated flow in the backfill.

Mesh Dependency

For Plaxis 2D the load-deflection curve for coarse and medium mesh gave about 7% overshoot compared to the very fine mesh. The medium, fine and very fine curves are very similar. The simulations stopped between 3 and 4,5 cm deformation due to numerical issues, and the failure loads were therefore not determined. Considering the results from Case 1 it is however expected that the failure loads for coarse and medium meshes would show the same overshoot as observed for smaller deformations, if the simulation went to failure.

In the Plaxis 3D simulation the coarse mesh displayed 7% overshoot compared to the fine mesh curve. The small differences are believed to be due to the coarse mesh having eight elements over the wall height, which makes it a relatively dense mesh. As previously shown for the 2D simulations in Case 1 and Case 2, the medium meshes display little overshoot compared to the very fine meshes because the medium mesh is dense enough to make as accurate calculations as those of the finer meshes. In other words the coarse mesh in this case has a high density, making it almost as accurate as the fine mesh.

Normal- and Shear Stresses

The normal stress distribution in figure 5.10 indicates a slightly curved stress distribution along the wall. The 10 kPa overshoot of the coarse mesh compared to the fine mesh is explained by the coarse mesh simulation being run further and none of the simulations reached the failure

load. If the failure load had been reached the curves are expected to have been more similar. The results indicate a horizontal stress of 30 kPa at the top of the wall. This makes sense due to the cohesion of the soil, which will allow for horizontal stresses to occur even if the vertical stress is zero.

The shear stress distribution in figure 5.11 indicates negative stresses from 0 to 1,2 meters depth and positive stresses from 1,2 to 1,7 meters, with the resultant shear force being approximately zero. This could lead to an apparent wall roughness $r = 0$.

Plaxis 2D and 3D Comparison

When comparing the Plaxis 2D and 3D results the curves in figure 5.19 are in good agreement. Considering the results from Case 1 the Plaxis 3D curve was expected to have a greater overshoot compared to the 2D curve, due to the mesh differences. The Plaxis 2D mesh has 18 elements over the wall height, compared to ten in Plaxis 3D. As previously mentioned the coarse, medium and fine mesh were found to provide very accurate results in the 3D simulation. Hence the mesh differences in 2D and 3D are believed to have little impact, as both meshes are dense enough to provide accurate results.

Hand Calculations

The calculated passive earth pressures in figure 5.21 indicate that the Rankine Theory is the best fit to the Plaxis results. The use of this theory was expected to give too low earth pressures, due to the theory's assumption of wall roughness $r = 0$. A reason for this could be that the Plaxis 2D simulation did not go to failure and the computed earth pressures could therefore be too small. On the other hand, due to the shear stresses in figure 5.11 being both negative and positive, the resultant shear force is approximately zero. This could lead to an apparent wall roughness $r = 0$. Assuming wall roughness of zero would indeed give a smaller K_P for the Janbu Theory, making it a better fit to the Plaxis results. The planar failure surface in Plaxis 2D supports the suspicion of apparent wall roughness being zero.

Chapter 6

Summary and Recommendation for Further Work

6.1 Summary and Conclusions

6.1.1 Summary of Literature Review

In this thesis the earth pressure theories developed by Rankine, Coulomb, Terzaghi and Janbu have been studied and used for hand calculations. The Rankine theory is the simplest method for calculating earth pressure, as its only variable is the friction angle ϕ, and it does not consider the roughness of the wall or the ground slope. The Coulomb theory is a bit more advanced, as it in addition to ϕ takes into account the roughness and the backfill slope. Both theories assume a plane failure surface, which is conservative. The Terzaghi and Janbu theories both assume a curved failure surface near the wall, making them more accurate. The biggest limitations of the theories is that they implicitly assumes that the dilatancy angle ψ is equal to the angle of friction ϕ, they do not account for the displacement of the wall, in addition to assuming linear horizontal stress distribution with depth.

6.1.2 Summary of Back-Calculations

This study has consisted of back-calculation of passive loading tests using the Mohr-Coulomb and Hardening Soil Model in Plaxis 2D and Plaxis 3D. Two passive load tests have been back-calculated in order to gather experience on soil behaviour during passive loading.

The results suggest that the stiffness parameters E' or E_{50}^{ref}, cohesion c_u or c and the friction angle ϕ are the most important parameters when modeling passive load tests in Plaxis. A critical evaluation of what values of ϕ to use is recommended, as sometimes the angle of friction as intepreted from the groups performing the tests tends to be too high. For the compacted gravel a value of 38° was found to be appropriate, and for the poorly compacted sand a value of 30° was used. For cases where the backfill is compacted, the use of empirical values in the higher range is recommended. For poorly compacted backfill empirical values in the lower range should be used. In the case of horizontal loading against gravel backfill surrounded by natural soil, the stiffness and shear strength of the surrounding soil was found to be important, while the stiffness of the gravel backfill was found to be less significant.

The author found that there is good agreement between the experimental load-deflection and the curves obtained from Plaxis 2D and 3D when the friction angle is adjusted to appropriate values for the backfill. In Case 1 the 3D simulations provided slightly more accurate results than the 2D simulations due to the 3D effects caused by the narrow concrete wall. For Case 2 the 2D and 3D simulations displayed equal accuracy, as the model had a 2D geometry that was extruded into a 3D model.

The mesh dependency was found to be varying for the two cases. In Case 1 the coarse mesh displayed a failure load overshoot of 12% compared to the very fine mesh, while the load-deflection curve in Case 2 had an overshoot of 7%. This is explained by the mesh differences, as the meshes in Case 1 had relatively low density compared to the meshes in Case 2. In both cases the simulations using medium, fine and very fine mesh provided similar results in Plaxis 2D. In the three dimensional simulations the difference in meshing caused big diversion for Case 1 while the Case 2 results were quite consistent. In Case 1 the coarse mesh curve displayed 20% overshoot compared to the fine mesh curve, while in Case 2 the overshoot was only 7%. This is explained by the difference in meshing for the two cases, as the coarse mesh in Case 2 was denser than that of Case 1. It is therefore recommended to review the different meshes before performing calculations, as sometimes the coarse mesh will be dense enough to provide nearly as accurate results as the fine mesh. The poor quality 10-node tetrahedral elements used in Plaxis 3D also

contributes to the overshoot of the failure load in the three dimensional calculations.

Hand calculations have been performed using the earth pressure theories of Rankine, Coulomb and Janbu. These results have been compared to the Plaxis 2D output and the results from the field tests. In the Case 1 the Janbu theory was in good agreement with the Plaxis results, while the Coulomb theory overestimated the passive earth pressures. The Rankine theory gave too low earth pressures due to the assumption of wall roughness $r = 0$. In the second case the resultant shear force acting on the wall was found to be approximately zero. This made the Rankine Theory the best fit, while the Coulomb and Janbu theories overestimated the passive earth pressure because a value of $r = 0,75$ was used in these calculations.

For simulation of wide bridge abutments with plane strain conditions the research suggests that Plaxis 2D should be used, preferably using a fine mesh which will provide accurate results. For more narrow abutments Plaxis 3D will be more relevant, and using a medium mesh is recommended. When using a medium mesh an overshoot in the range of 5 to 10% is expected.

6.2 Recommendation for Further Work

For bridge abutments in Norway the most commonly used backfill is gravel, and the abutments are often narrow. For further investigations it would be interesting to study the 3D effects of real abutment designs. The 3D effects can result in a considerable increase in passive resistance compared to the oversimplification of 2D, which is often used in design. To what degree a 3D simulation might overshoot the real failure load due to poor elements and a too coarse mesh should also be studied further. Cases with gravel backfill is believed to be the most relevant. It would also be beneficial to back-calculate experiments where the stresses behind the wall have been measured for comparison.

In this thesis only the Hardening Soil Model was used when modeling the backfill materials. It would be interesting to also use other material models in the back-calculations for comparison.

List of Figures

List of Tables

Bibliography

Aarhaug, O. R. (1984). In *Geoteknikk og fundamentering 2, kap 5*. NKI-forlaget.

Bell, K. (2013). *An engineering approach to Finite Element Analysis of linear structural mechanics problems*. Fagbokforlaget. ISBN: 978-82-321-0268-6.

Clough, R. W., Turner, M. J., Martin, H. C., and Topp, L. (1956). Stiffness and deflection analysis of complex structures. *Journal of the Aeronautical Sciences*, 23(9).

Coulomb, C. A. (1776). Essai sur une application des regles de maximis minimis a quelques problemes de statique, relatifs a l'architecture. volume 7. Paris: De l'Imprimerie Royale.

Duncan, J. and Mokwa, R. (2001). Passive earth pressures: Theories and tests. *Journal of Geotechnical and Geoenvironmental Engineering*, 127(3):248–257. doi:10.1061/(ASCE)1090-0241(2001)127:3(248).

Emdal, A., Grande, L., and Nordal, S. (2015). *Compendium in TBA 5100 Theoretical Soil Mechanics*. NTNU.

Fang, Y., Chen, T., and Wu, B. (1994). Passive earth pressures with various wall movements. *Journal of Geotechnical and Geoenvironmental Engineering*, 120(8):1307–1323. doi:10.1061/(ASCE)0733-9410(1994)120:8(1307).

Fang, Y., Ho, Y., and Chen, T. (2002). Passive earth pressure with critical state concept. *Journal of Geotechnical and Geoenvironmental Engineering*, 128(8):651–659. doi:10.1061/(ASCE)1090-0241(2002)128:8(651).

Janbu, N. (1972). Earth pressure computations in theory and practice. *5th European Conference on Soil Mechanics and Found. Engineering*, 1.

Kowalska, M. (2015). Influence of the ratio between dilatancy angle and internal friction angle on stress distribution between a gravity retaining wall. *Architecture Civil Engineering Environment No. 1/2015*.

Magar, A. (2016). Earthquake response of different types of retaining walls. Master's thesis, NTNU.

Mathisen, K. M. (2017). Lecture notes from tkt4192 elementmetoden i styrkeanalyse. ntnu. week 1, 2017.

Matsuzava, H. and Hazarika, H. (1996). Analyses of of active earth pressure against rigid retaining wall subjected to different modes of movement. *Soils and foundations*, 36(3):51–65. doi:10.3208/sandf.36.3 51.

Nordal, S. (2017). *Lecture notes and background material in TBA4116 Geotechnical Engineering Advanced Course*. NTNU.

Plaxis (2017). *Plaxis 3D Reference Manual 2017*.

Plaxis (2018). *Plaxis 2D Reference Manual 2018*.

Rankine, W. J. M. (1857). On the stability of loose earth. *Philosophical Transactions of the Royal Society of London*, 147:9–27. doi:10.1098/rstl.1857.0003.

Rhodes, S. (2001). Integral bridges and the modelling of soil structure interaction. http://www.academia.edu/29713086.

Schanz, T. (1998). On the mechanical behavior of frictional material. *Mitteilung 45 des Instituts fur Geotechnik, University of Stuttgart, Stuttgart, Germany.*

Shamsabadi, A. and Nordal, S. (2006). Modeling passive earth pressure on bridge abutments for nonlinear seismic soil - structure interaction using plaxis. *Plaxis Bulletin*, 20:8–14. https://www.plaxis.com/content/uploads/2016/10/Plaxis-Bulletin-20.pdf.

Terzaghi, K. (1943). *Theoretical Soil Mechanics. Chapter 2 pages 51-65.* John Wiley and Sons, New York.

Terzaghi, K., Peck, R. B., and Mezri, G. (1996). *Soil Mechanics in Engineering Practice 3rd edition.* John Wiley and Sons, New York.

Vegdirektoratet (2014). *Statens Vegvesen Håndbok V220 Geoteknikk i vegbygging*.

Vermeer, P., Schanz, T., and Bonnier, P. (1999). The hardening soil model: Formulation and verification. *Beyond 2000 in Computational Geotechnics - 10 years of PLAXIS*.

Wilson, P. and Elgamal, A. (2010). Large-scale passive earth pressure load-displacement tests and numerical simulation. doi:10.1061/(ASCE)GT.1943-5606.0000386.

Appendix A

Additional Information for Case 1

A.1 Hand calculations Case 1

A.1.1 Rankine Theory

Natural soil

$$K_p = tan^2(45^\circ + \frac{\phi}{2}) = tan^2(45^\circ + 0) = 1 \tag{A.1}$$

$$K_A = tan^2(45^\circ - \frac{\phi}{2}) = tan^2(45^\circ - 0) = 1 \tag{A.2}$$

$$p_p = p_v K_p + 2c\sqrt{K_p} = p_v + 2s_u = 11kPa + 2 \cdot 47kPa = 105kPa \tag{A.3}$$

$$P_p = p_p \cdot A = 105kPa \cdot 1,1m \cdot 1,9m = 219kN \tag{A.4}$$

$$p_A = p_v K_A - 2c\sqrt{K_A} = p_v - 2s_u = 11kPa - 2 \cdot 47kPa = -83kPa \tag{A.5}$$

$$P_A = p_A \cdot A = -83 \cdot 1,1m \cdot 1,9m = -173kPa \tag{A.6}$$

$$P_{total} = P_P - P_A = 219kN - (-173kN) = 392kN \tag{A.7}$$

$$\delta = \epsilon \cdot 2H = \frac{\sigma}{E} \cdot 2H = \frac{105kPa}{40000kPa} \cdot 2 \cdot 1,1m = 2,625 \cdot 10^{-3} \cdot 2 \cdot 1,1 = 5,8mm \tag{A.8}$$

Natural Soil with Gravel Backfill

$$K_p = tan^2(45^\circ + \frac{\phi}{2}) = tan^2(45^\circ + \frac{35^\circ}{2}) = 3,7 \tag{A.9}$$

$$K_A = tan^2(45^\circ - \frac{\phi}{2}) = tan^2(45^\circ - 0) = 1 \tag{A.10}$$

$$p_p = p_v \cdot K_p = 11,5kPa \cdot 3,7 = 43kPa \tag{A.11}$$

$$P_P = p_p \cdot A = 43kPa \cdot 1,1m \cdot 1,9m = 90kN \tag{A.12}$$

$$p_A = p_v K_A - 2c\sqrt{K_A} = p_v - 2 \cdot s_u = 11kPa - 2 \cdot 35kPa = -59kPa \tag{A.13}$$

$$P_A = p_A \cdot A = -59kPa \cdot 1,1m \cdot 1,9m = -123kN \tag{A.14}$$

$$P_{total} = P_P - P_A = 90kN - (-123kN) = 213kN \tag{A.15}$$

$$\delta = \epsilon \cdot 2H = \frac{\sigma}{E} \cdot 2H = \frac{43kPa}{33000kPa} \cdot 2 \cdot 1,1m = 1,303 \cdot 10^{-3} \cdot 2 \cdot 1,1 = 2,9mm \tag{A.16}$$

A.1.2 Coulomb Theory

Natural Soil

$$tan\delta = R_{int} tan\phi = 0,75 \cdot tan(0) = 0 \rightarrow \delta = 0 \tag{A.17}$$

$$\begin{aligned} K_P &= \frac{sin^2(\alpha - \phi')}{sin^2(\alpha) \cdot sin(\alpha + \delta) \cdot (1 - \sqrt{\frac{sin(\phi' + \delta) \cdot sin(\phi' + \beta)}{sin(\alpha + \delta) \cdot sin(\alpha + \beta)}})^2} \\ &= \frac{sin^2(90 - 0)}{sin^2(90) \cdot sin(90 + 0) \cdot (1 - \sqrt{\frac{sin(0+0) \cdot sin(0+0)}{sin(90+0) \cdot sin(90+0)}})^2} = 1 \end{aligned} \tag{A.18}$$

$$K_A = \frac{sin^2(\alpha+\phi')}{sin^2(\alpha)\cdot sin(\alpha-\delta)\cdot(1+\sqrt{\frac{sin(\phi'+\delta)\cdot sin(\phi'-\beta)}{sin(\alpha-\delta)\cdot sin(\alpha+\beta)}})^2} = \frac{sin^2(90+0)}{sin^2(90)\cdot sin(90-0)\cdot(1+\sqrt{\frac{sin(0+0)\cdot sin(0-0)}{sin(90-0)\cdot sin(90+0)}})^2} = 1 \tag{A.19}$$

$$p_P = p_v K_P + 2c\sqrt{K_A} = p_v + 2s_u = 11kPa + 2\cdot 47kPa = 105kPa \tag{A.20}$$

$$P_P = p_P \cdot A = 105kPa \cdot 1,1m \cdot 1,9m = 219kPa \tag{A.21}$$

$$P_{under} = s_u \cdot R_{int} \cdot A = 47kPa \cdot 0,75 \cdot 1,9m \cdot 0,9m = 60kN \tag{A.22}$$

$$p_A = p_v K_A - 2c\sqrt{K_A} = p_v - 2s_u = 11kPa - 2\cdot 47kPa = -83kPa \tag{A.23}$$

$$P_A = p_A \cdot A = -83 \cdot 1,1m \cdot 1,9m = -173kPa \tag{A.24}$$

$$P_{total} = P_P - P_A + P_{under} = 219kN - (-173kN) + 60kN = 452kN \tag{A.25}$$

$$\delta = \epsilon \cdot 2H = \frac{\sigma}{E}\cdot 2H = \frac{219kPa}{40000kPa}\cdot 2\cdot 1,1m = 5,475\cdot 10^{-3}\cdot 2\cdot 1,1 = 12mm \tag{A.26}$$

Natural Soil with Gravel Backfill

$$tan\delta = R_{int} tan\phi = 0,75\cdot tan(35^\circ) = 0,53 \rightarrow \delta = 28^\circ \tag{A.27}$$

$$K_p = \frac{sin^2(\alpha-\phi')}{sin^2(\alpha)\cdot sin(\alpha+\delta)\cdot(1-\sqrt{\frac{sin(\phi'+\delta)\cdot sin(\phi'+\beta)}{sin(\alpha+\delta)\cdot sin(\alpha+\beta)}})^2} = \frac{sin^2(90-35)}{sin^2(90)\cdot sin(90+28)\cdot(1-\sqrt{\frac{sin(35+28)\cdot sin(35+0)}{sin(90+28)\cdot sin(90+0)}})^2} = 13,3 \tag{A.28}$$

$$K_A = \frac{sin^2(\alpha+\phi')}{sin^2(\alpha)\cdot sin(\alpha-\delta)\cdot(1+\sqrt{\frac{sin(\phi'+\delta)\cdot sin(\phi'-\beta)}{sin(\alpha-\delta)\cdot sin(\alpha+\beta)}})^2} = \frac{sin^2(90+0)}{sin^2(90)\cdot sin(90-0)\cdot(1+\sqrt{\frac{sin(0+0)\cdot sin(0-0)}{sin(90-0)\cdot sin(90+0)}})^2} = 1 \tag{A.29}$$

$$p_p = p_v K_p + 2c\sqrt{K_p} = p_v \cdot K_p = 11,5kPa \cdot 13,3 = 153kPa \tag{A.30}$$

$$P_P = p_p \cdot A = 153kPa \cdot 1,1m \cdot 1,9m = 320kN \tag{A.31}$$

$$P_{under} = s_u \cdot R_{int} \cdot A = 35kPa \cdot 0,75 \cdot 1,9m \cdot 0,9m = 45kN \tag{A.32}$$

$$p_A = p_v K_A - 2c\sqrt{K_A} = p_v - 2s_u = 11kPa - 2 \cdot 35kPa = -59kPa \tag{A.33}$$

$$P_A = p_A \cdot A = -59 \cdot 1,1m \cdot 1,9m = -123kPa \tag{A.34}$$

$$P_{total} = P_P - P_A + P_{under} = 320kN - (-123kN) + 45kN = 448kN \tag{A.35}$$

$$\delta = \epsilon \cdot 2H = \frac{\sigma}{E} \cdot 2H = \frac{153kPa}{33000kPa} \cdot 2 \cdot 1,1m = 4,64 \cdot 10^{-3} \cdot 2 \cdot 1,1 = 10,2mm \tag{A.36}$$

A.1.3 Janbu Theory

Natural Soil

Roughness $r = R_{int} = 0,75$ is assumed, giving $\kappa = 2,5$ using Janbu's chart for s_u analysis. The passive earth pressure is given by equations A.37 and A.38:

$$p_p = p_v + \kappa \cdot \tau_c = p_v + \kappa \cdot s_u = 11kPa + 2,5 \cdot 47kPa = 129kPa \tag{A.37}$$

$$P_p = p_p \cdot A = 129kPa \cdot 1,1m \cdot 1,9m = 270kN \tag{A.38}$$

A horizontal shear force is acting underneath the concrete block:

$$P_{under} = s_u \cdot R_{int} \cdot A = 47kPa \cdot 0,75 \cdot 1,9m \cdot 0,9m = 60kN \tag{A.39}$$

Assuming suction in the soil on the right side of the concrete block, the active earth pressure is given by equations A.40 and A.41:

$$p_A = p_v - \kappa \cdot \tau_c = p_v - \kappa \cdot s_u = 11kPa - 2,5 \cdot 47kPa = -107kPa \tag{A.40}$$

$$P_A = p_A \cdot A = -107kPa \cdot 1,1m \cdot 1,9m = -224kN \tag{A.41}$$

This gives a resulting horizontal force P_{total}:

$$P_{total} = P_p - P_A + P_{under} = 270kN - (-224kN) + 60kN = 554kN \tag{A.42}$$

Horizontal displacement at failure:

$$\delta = \epsilon \cdot 2H = \frac{\sigma}{E} \cdot 2H = \frac{129kPa}{40000kPa} \cdot 2 \cdot 1,1m = 3,225 \cdot 10^{-3} \cdot 2 \cdot 1,1 = 7,1mm \tag{A.43}$$

Natural Soil with Gravel Backfill

$r = R_{int} = 0,75$ and $\phi = 35°$ is assumed, giving $K_P = 7$. Attraction $a = 0$ is assumed.

Passive earth pressure:

$$p'_p + a = K_p(p'_v + a) \rightarrow p'_p = 7 \cdot 11,5kPa = 80kPa \tag{A.44}$$

$$P'_P = p'_p \cdot A = 80kPa \cdot 1,1m \cdot 1,9m = 167kN \tag{A.45}$$

Horizontal shear force acting underneath the concrete block:

$$P_{under} = s_u \cdot R_{int} \cdot A = 35kPa \cdot 0,75 \cdot 1,9m \cdot 0,9m = 45kN \tag{A.46}$$

Active earth pressure, assuming suction:

$$p_A = p_v - \kappa \cdot \tau_c = p_v - \kappa \cdot s_u = 11kPa - 2,5 \cdot 35kPa = -76,5kPa \tag{A.47}$$

$$P_A = p_A \cdot A = -76,5kPa \cdot 1,1m \cdot 1,9m = -160kN \tag{A.48}$$

Total horizontal force:

$$P_{total} = P'_P - P_A + P_{under} = 167kN - (-160kN) + 45kN = 372kN \tag{A.49}$$

Horizontal displacement at failure:

$$\delta = \epsilon \cdot 2H = \frac{\sigma}{E} \cdot 2H = \frac{80kPa}{35000kPa} \cdot 2 \cdot 1,1m = 5mm \tag{A.50}$$

A.2 More Details

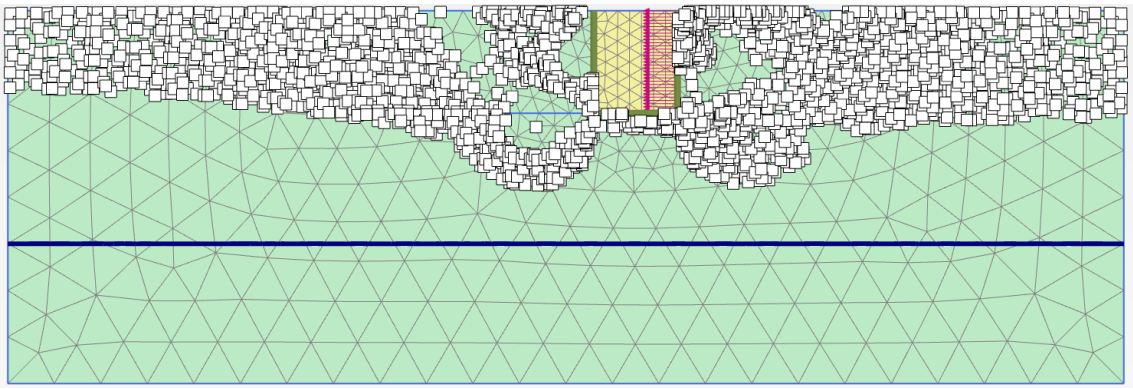

Figure A.1: Tension cut-off points for natural soil

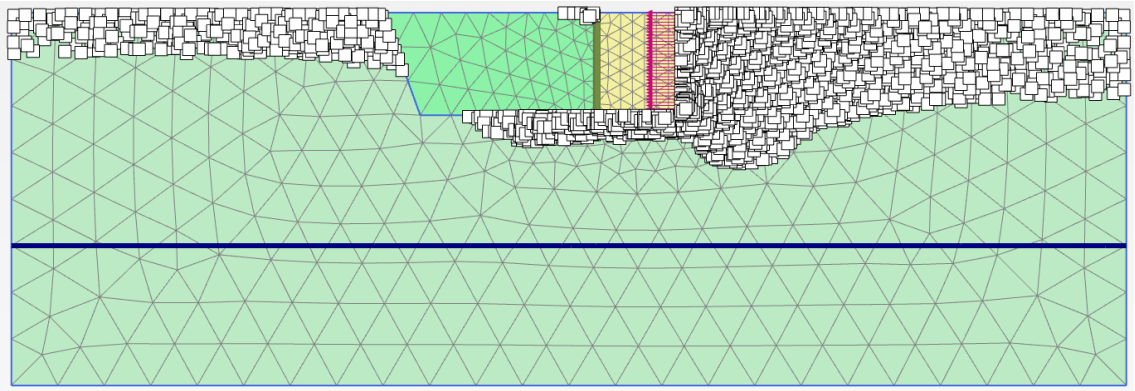

Figure A.2: Tension cut-off points for natural soil with gravel backfill

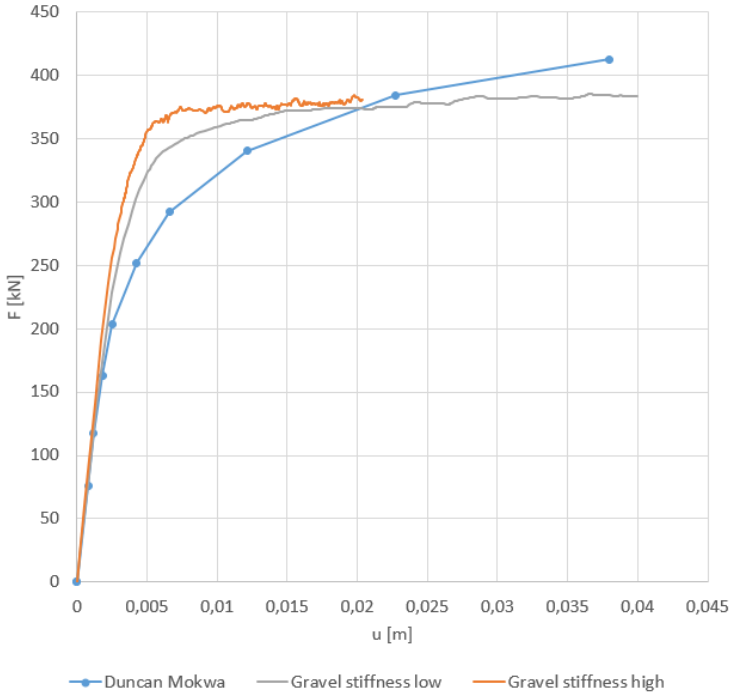

Figure A.3: Load deflection curves for varying E_{50}^{ref} for gravel backfill

Appendix B

Additional Information for Case 2

B.1 Hand Calculations for Case 2

B.1.1 Rankine Theory

$$K_p = tan^2(45^\circ + \frac{\phi}{2}) = tan^2(45^\circ + \frac{30^\circ}{2}) = 3 \tag{B.1}$$

$$p_p = p_v \cdot K_p + 2c\sqrt{K_p} = 17,3kPa \cdot 3 + 2 \cdot 6kPa \cdot \sqrt{3} = 72kPa \tag{B.2}$$

$$P_P = p_p \cdot A = 72kPa \cdot 1,68m \cdot 2,74m = 331kN \tag{B.3}$$

$$\delta = \epsilon \cdot 2H = \frac{\sigma}{E} \cdot 2H = \frac{72kPa}{30000kPa} \cdot 2 \cdot 1,68m = 2,4 \cdot 10^{-3} \cdot 2 \cdot 1,68m = 8,1mm \tag{B.4}$$

B.1.2 Coulomb Theory

$$tan\delta = R_{int} tan\phi = 0,75 \cdot tan(30^\circ) = 0,43 \rightarrow \delta = 23^\circ \tag{B.5}$$

$$K_p = \frac{sin^2(\alpha - \phi')}{sin^2(\alpha) \cdot sin(\alpha + \delta) \cdot (1 - \sqrt{\frac{sin(\phi' + \delta) \cdot sin(\phi' + \beta)}{sin(\alpha + \delta) \cdot sin(\alpha + \beta)}})^2} = \frac{sin^2(90 - 30)}{sin^2(90) \cdot sin(90 + 23) \cdot (1 - \sqrt{\frac{sin(30+23) \cdot sin(30+0)}{sin(90+23) \cdot sin(90+0)}})^2} = 7 \tag{B.6}$$

$$p_p = p_v K_p + 2c\sqrt{K_p} = p_v \cdot K_p = 17,3kPa \cdot 7 + 2 \cdot 6kPa \cdot \sqrt{7} = 153kPa \tag{B.7}$$

$$P_P = p_p \cdot A = 153kPa \cdot 1,68m \cdot 2,74m = 704kN \tag{B.8}$$

$$P_{total} = P_P = 704kN \tag{B.9}$$

$$\delta = \epsilon \cdot 2H = \frac{\sigma}{E} \cdot 2H = \frac{153kPa}{30000kPa} \cdot 2 \cdot 1,68m = 5,1 \cdot 10^{-3} \cdot 2 \cdot 1,68 = 17,1mm \tag{B.10}$$

B.1.3 Janbu Theory

$r = R_{int} = 0,75$ and $\phi = 30°$ is assumed, giving $K_P = 4,5$. Attraction a = 6 kPa is assumed.

$$p'_p + a = K_p(p'_v + a) \rightarrow p'_p = 4,5 \cdot (17,3kPa + 6kPa) - 6kPa = 99kPa \tag{B.11}$$

$$P'_P = p'_p \cdot A = 99kPa \cdot 1,68m \cdot 2,74m = 455kN \tag{B.12}$$

$$P_{total} = P'_P = 455kN \tag{B.13}$$

$$\delta = \epsilon \cdot 2H = \frac{\sigma}{E} \cdot 2H = \frac{99kPa}{30000kPa} \cdot 2 \cdot 1,68m = 11,1mm \tag{B.14}$$